LOUGHBOROUGH UNIVERSITY

Invariant Manifolds Mediating Collinear Hydrogen Exchange Reaction

by

Mohammed Alharthi

A DOCTORAL THESIS
submitted in partial fulfillment of the requirements
for the degree of Doctor of Philosophy
of Loughborough University

in the
Faculty of Science
Department of Mathematical Sciences

November 2019

Declaration of Authorship

I, Mohammed Alharthi, declare that this thesis titled, "Invariant Manifolds Mediating Collinear Hydrogen Exchange Reaction "and the work presented in it are my own. I confirm that:

- This work was done wholly or mainly while in candidature for a research degree at Loughborough University.
- Where any part of this thesis has previously been submitted for a degree or any other qualification at Loughborough University or any other institution, this has been clearly stated.
- Where I have consulted the published work of others, this is always clearly attributed.
- Where I have quoted from the work of others, the source is always given. With the exception of such quotations, this thesis is entirely my own work.
- I have acknowledged all main sources of help.
- Where the thesis is based on work done by myself jointly with others, I have made clear exactly what was done by others and what I have contributed myself.

Signed:

Date: **November 2019**

"Logic is the foundation of the certainty of all knowledge we acquire."

Leonhard Euler

LOUGHBOROUGH UNIVERSITY

Abstract

Faculty of Science, Department of Mathematical Sciences

by Mohammed Alharthi

We discuss the phase space structure for the collinear hydrogen exchange system crosses an energy barrier. Above the reaction threshold, the system must pass through a Symmetric Stretch Periodic Orbit (SSPO) where the dynamics are structuring a Dividing Surface (DS), that separates reactants and products. At low energy, the SSPO can serve as a dividing surface that satisfies the no-recrossing assumption of Transition State Theory (TST). As the energy increases, saddle-node bifurcations occur on both sides of the SSPO. Above the bifurcation energy, trajectories appear that recross the central DS. The region of recrossing trajectories is bounded by the stable manifolds of the additional Unstable Periodic Orbits (UPOs). We investigate the fractal structure of the TST violating islands of the DS and how it is determined by the invariant manifolds of the additional periodic orbits. We demonstrate that the various layers are all bounded by the same stable manifold.

The second part is devoted to the study of the phase space structure in a region where the stable manifold initiated. It appears that some of the ensemble trajectories do not cross the DS. We demonstrate the area of those trajectories validating the boundary of various layers from those trajectories that do not. Following this, we make use of the symmetry and demonstrate that these various layers appeared on all versions of the DS and are bounded by the symmetric invariant manifolds belonging to the UPOs, which existed on both sides of the SSPO. Finally, we demonstrate those invariant manifolds intersecting each other, before intersecting the DS, which leads to more complicated behaviour.

Keywords:

Transition state theory, Hamiltonian, dividing surface, NHIM, centre manifold, reactive island, stable and unstable cylindrical manifolds.

Acknowledgements

I would like to express my sincere gratitude to: My advisor, Dr Thomas Bartsch, for the continuous support of my study and research, for his patience, motivation, enthusiasm, and immense knowledge. His guidance helped me in all the time of research and writing of this research. I am grateful to my sponsor Taif University and the Ministry of Higher Education of Saudi Arabia from whom I get financial support during my study in the UK.

I am also thankful to my wife Foz for her constant support and her patient. My lovely children give me so much joy and love during my stay in the UK and deserve more in return. I will never forget my dad who took the lead to heaven before the completion of this work and my mother who encourage and pray for me throughout the time of my research. I am always grateful to my parents.

I would like to thank the school of Mathematical science at Loughborough University for their support.

Contents

List of Figures

List of Tables

Abbreviations

TST	**T**ransition **S**tate **T**heory
PODS	**P**eriodic **O**rbit **D**ividing **S**urface
NHIM	**N**ormally **H**yperbolic **I**nvariant **M**anifold
dof	**d**egree **o**f **f**reedom
SSPO	**S**ymmetric **S**tretch **P**eriodic **O**rbit
F_1	**C**ollinear **P**eriodic **O**rbit
F_1'	**C**ollinear mirror image **P**eriodic **O**rbit
RI	**R**eactive **I**sland
UPO	Collinear **U**nstable **P**eriodic **O**rbit
H1, H2, H3	refer to three Hydrogen atoms

To my family...

Chapter 1

Introduction

Shrink to the size of a hydrogen atom and journey with us to the core of the hydrogen molecule exchange reaction. Using mathematical models and physical meaning, you can travel where no one predicts before. Explore how the exchange happens in a Hamiltonian system where the trajectories move inside tubes and the energy used to turn one atom of the molecule by another one with similar structure and mass weight—producing new molecule, but it is the only hydrogen.

The hydrogen exchange reaction leads us to study the phase-space structure behind the exchange dynamics in a system inherited vibration. In this work, we investigate the fractal structure of the dynamics, forming a phase space object in terms of transformation between two distinct regions in phase space. As you might know with the massless weight of the hydrogen a little goes unwell as higher energy needed to break the existing bond and a new one is born. Despite the fact, the hydrogen is a quantum atom, quantum effects (see, e.g. [1]and [2]) such as tunnelling and threshold behaviour are put aside from classical points of view. Tunnelling along the reaction coordinates makes the quantum reaction more complicated even in 1 dof system [3]. The classical TST provides the conceptional idea of separability, which is the basis of all attempts to produce the TST quantum version [4]. The realisation of classical TST also has consequences in quantum progress which should reduce the problem to the classical limitation in order to have all classical computational benefits. We study here a classical particle

crossing an energetic barrier with enough energy above the reaction threshold. Again if one widens the threshold barrier or increase the height beyond the barrier energy, it will have no consequence in the classical sense because it is less likely for a particle with just right enough energy to make a reaction. Moreover, if one tries to substitute a hydrogen atom by a heavier atom such as deuteration [5, 6], the structure of the system will then dramatically change to an asymmetric system that is not the key focus of this research. Something is also to think about when a hydrogen atom perhaps meets with the hydrogen molecule on a top of a potential energy barrier.

The hydrogen exchange reaction requires some knowledge on the potential energy surface corresponding to the interaction of the hydrogen atoms. This surface has been investigated and developed for both classical and quantum mechanics. In the past, the rate's calculation is based on the absolute rate theory[7], where the surface highly needed in the neighbourhood of the activated complex in configuration space. A priori treatment[8]–[9] provided limited detail for the Boys and Shavitt [10] configurations of the hydrogen reaction in order to obtain a semi-empirical expression for the PES, which was not accurate for application. The best approach is based on the London equation [11] and used by Eyring Polanyi and others for estimating the reaction rate. The Eyring potential surface appeared to neither adequate enough nor agreed with all prior approaches. Although, a vital modification proposed by Sato [12], The Eyring –Sato potential is less accurate for nonlinear configurations as the central atom is neglected. The refinement of the Eyring–Polanyi approach and Sato potential energy results in the Porter–Karplus surface [13], which developed classically for especially symmetric configuration of the hydrogen.

However, another analytical column approach developed from Truhlar and Horowitz approach [14] in order to yield an accurate analytic formulation which was carried out by Liu and Siegbahn [15]. On similar *ab initio* method, the Varanadas potential [16] provided a less accurate rate for the hydrogen reaction. These surfaces were fitted depending on the number of energies values conformation which have been used by many research group(see, e.g. [17],[18])for both quantum and quasi-classical trajectory calculations. New modification needed to extend the earlier results to more higher

energies. Recent development and progress made to obtain the Boothroyd, Keogh, Martin, and Peterson (BKMP) potential surface [19] which is in agreement with the classical Porter–Karplus potential in terms of critical point's position and energy value in the collinear case. Recently, Iñarrea *et al* [20] used both surfaces in the bifurcation of dividing surfaces study and found that their bifurcation diagrams differ.

The Transition State Theory (TST) [1, 21–26] provides an insightful guide to study the dynamics of the chemical reaction by providing a fundamental picture of reactants and products regions that are kept apart by a barrier. For that, the TST assumes to locate a Dividing Surface (DS) in the neighbourhood of the barrier that could be a saddle point. The system must pass the DS through a bottleneck which can be unstable periodic orbit in a particular case. The existence of the unstable periodic orbit in the region around the saddle point can be used to connect two chemical regions in configuration space where the reaction occurs, and the rate is determined. Because crossing the saddle point is the slowest step in the reaction process and for this reason, one can define the reaction rate as the number of systems that cross the DS in unite time proportional to the population of the reactant region. TST proves that surface can give an exact rate if it is recrossing free, which means one reaction per time. As a result, the reaction rate is proportional to the total flux of reactive trajectories on the DS. Something also is to think about, what consequences to the rate if the DS is recrossed?

In the 1970s, the TST reached the peak of its revolution in practice, when the collinear hydrogen exchange reaction and its evolution adopted ideas of the TST to calculate the rate. Such developments perform vital tools including the Poincare Surface of Section (PSS) which can be seen, for example, in [27, 28]. Due to the simplicity, the TST provides an accurate reaction rate for the collinear case, up to specific energy. Beyond that energy, when higher energy is applied, it becomes inaccurate rather quickly.

In 1973, Pechukas *et al* [29] found a simple standard for the collinear rate to be exact, in terms of the TST, for a range of energies. It was observed that almost all trajectories crossed a DS only once, up to a particular energy value, where some trajectories, associated near the potential barrier, recross the DS. This region is where all the atoms collide into a complex, and the only possible explanation of the TST failure is called a

"collision complex ". The existence of the collision complex was not clearly explained, including its cause and connection to the reaction rate. It was not until 1978, Pollak and Pechukas found that the unstable periodic orbit vibrated between two equipotential and thus explained how the collision complex came into existence. The projection of the unstable periodic orbit determines the optimal Periodic Orbit Dividing Surface (PODS) which solved the problem of recrossing in phase space as shown by Pechukas, Pollak and McLafferty [30]. The new finding regarding the unstable periodic orbits is used to construct the DS through which the flux passes the transition state (TS).

In contrast, the TST is based on a single TS, through which the rate is proportional to the flux. However, when studying the hydrogen exchange reaction, multiple (unstable) periodic orbits were considered by Pechukas *et al* [31] in 1978. By using this, a new strategy was formed for a better transition state in connection with the best accuracy rate calculated, called the Variational Transition State Theory (VTST) [32] such that the transition state would not necessarily have to be at the saddle point. The new VTST approach shows a more accurate rate and can be applied to higher energy values. However, if there were more than one PODS, Pechukas *et al* [33] - [30] declared that TST would break down. Therefore, the reaction rate will be proportional to that PODS minimises the flux.

Unfortunately, All PODS can be recrossed at a range of higher energy values during the reaction and also nonreactive trajectories start to appear in the DS, which overestimates the reaction rate. In this work, we focus on the initial conditions structuring the DS and address such a change in phase space structure would lead to a change in the DS and pay attention to the dynamical effect due to recrossing in a system with two degrees of freedom (dof). This system inherits a simple configuration such that their hydrogen atoms are confined to move on a line. As you may know, if the dynamics transit from regular to chaotic, the system will be subject to chaotic behaviour leading to a proper challenge. Because propagating trajectories with slightest small deviation may yield to a qualitatively different evolution, such information has raised many questions regarding transport that have remained active. Does computing processing meet an advance theory that has been already developed for studying even more chaotic systems?

Since then, the original idea of the PODS was well explained in configuration space and soon recognised that a proper DS must be defined in phase space. Using an advanced dynamical theory, concerning the role of invariant manifolds of the PODS, Davis [34] showed how to partition the phase space. Only later on the 1990s, the PODS is replaced by a Normally hyperbolic invariant manifold (NHIM) which represent a higher–dimensional saddles associated with separatrices. Wiggins [35] has shown how to construct the NHIM in phase space in the 1990s. This follows by normal form theory that helps to obtain such a DS in the early 2000s [36]. However, even after these advances in the theory, the optimal DS can be found in practice in a lower dimension than the three-dimensional phase space. Therefore, the TST has to wait for further development in multidimensional dynamical theory. In the past, neither the computer power was adequate to meet theoretical understanding in order to explore the phase space structure beyond two degrees of freedom [37].

For two degrees of freedom, the Symmetric Stretch Periodic Orbit (SSPO) living in the vicinity of the saddle point is the best-suited candidate for the DS. Allahem *et al* [38] have recently studied if the SSPO preserves its normally hyperbolic property, which means the contraction and expansion rate transversed to it will persist under small perturbations. They called it the central sphere due to the breakdown of the normal hyperbolicity. They also stated that among several periodic orbits within region of the saddle point, the SSPO is the only periodic orbit violate the normal form hyperbolicity conditions. These conditions have two main implications: first, the dynamical structure of the periodic orbit will persist under perturbations, such as energy values change. Secondly, the periodic orbit is attached to the stable and unstable invariant manifolds. These manifolds distinguish between reactive and nonreactive trajectories in phase space where trajectories are invariant in a sense no trajectory cross other ones. They also channel the flux from the reactant through the DS and on into the product side. Nevertheless, the symmetric stretch periodic orbit undergoes a sequence of bifurcations in which loses and regains its stability. This kind of information allows a detailed description to the reaction dynamic that goes well beyond reaction rate calculations [39]–[40].

This study is an extension to recent work which provides pathways and insightful guide to the current research. With the help of the previous study, we can figure out the bifurcation where the system admits several periodic orbits. Of which we are looking for the unstable periodic orbit held stationary flux and change the structure significantly in phase space. There are few periodic orbits in the collinear reaction at higher energy as found by Iñarrea *et al* [20]. These additional stable and unstable periodic orbits occur symmetrically at the first bifurcation where the SSPO is dominant. Recently, Allahem [41] hypothesised that nonreactive trajectories are separated from reactive trajectories by invariant manifolds associated with the collinear unstable periodic orbit (UPO).

In this thesis, we use the collinear $H + H_2$ reaction as an example to confirm that the UPO can change the standard transition structure. This periodic orbit shall have an impact to destroy the TST rate calculation at a specific energy E above the bifurcation energy. The emergence of nonreactive islands on the central PODS coincides with the stable and unstable manifolds of the UPO intersect each other in the product side. Our main goal is to determine these manifolds and explain in more detail their qualitatively influence to the dynamics which are known to be chaotic at higher energy.

Knowledge of the previous works helps us to determine the manifolds mostly responsible for the breakdown transition structure and to make use for comparison. We know that the transition is simple in a small range of energies above the threshold for the collinear reaction. As energy increases, nonreactive islands of the DS start to appear as a sign to the complexity of the Hamiltonian dynamics. The TST rate for the collinear hydrogen was calculated by Pechukas and McLaffery[21, 29] and then improved by Miller *et al* [2, 42] who calculated the reaction rate for the collinear hydrogen and found that the TST is exact up to higher energy. Most recently, Iñarrea [20] used the Porter-Karplus potential energy [13] to find the TST fails at about 0.2 above the barrier. The potential energy function is mainly calculated several times (e.g. [19]) and used for the purpose of this thesis. Beyond that, Iñarrea *et al* [20] have studied the bifurcations of the PODS, and the NHIM were discussed in [43, 44] for the collinear and full dynamics as well. Allahem and Bartsch [38] found that the breakdown of the NHIM is not the

reason for TST failure. Moreover, they state that the additional collinear periodic orbit emerged from the bifurcation of the symmetric stretch periodic orbit causes complexity in phase space.

The purpose of this thesis is divided into two main parts: we first confirm the previous result demonstrated by Allahem [41]. He proves that the stable manifold of the UPO bound the main nonreactive layer on the DS. He claimed that the stable manifold of the UPO intersects the DS at the boundary of the first nonreactive islands at a specific high energy value just above the bifurcation. Hereafter, we study his finding via an invariant property that is the basis of any dynamical study. We also describe qualitatively how the UPO with its separatrix branches cause these nonreactive droplets to open up in the DS. In addition to that, we make use of the symmetry properties inherited in the system to find that manifold related to the mirror image of the UPO in terms of the boundary of nonreactive islands on the DS. In the second part, we study the chaotic scattering near the UPO to determine the area associated with all the boundaries related to those nonreactive layers on the DS. Our main aim is to find how these regions transit to chaos in a system known to be regular at low energy. Our approach demonstrates the stable and unstable manifolds of the UPO mainly to show their heteroclinic intersections which cause the transition structure in the central PODS. These manifolds intersect the DS from the product side where only the stable manifold bounds the nonreactive layers projected in the forward hemisphere. Such chaotic behaviour is now understood when the system undergoes homoclinic tangent bifurcation.

The contents of this thesis start with background material regarding the formation of the TST explained in Chapter 2. There, we give a brief overview of the Hamiltonian system and the TST reaction rate, which is not computed herein. We also describe how the transition structure layout in phase space that is primarily centred in configuration space. This includes some necessary information on how to construct the DS where a periodic orbit gives a minimum flux through cylindrical manifolds existed in phase space. We study the stability of periodic orbit that shall cause the breakdown of the DS configuration. In chapter 3, the hydrogen exchange reaction is used as a practical model to describe the Hamiltonian collinear system within the vicinity of the saddle point.

We focus on the collinear case by giving extra details, including previous knowledge that show gaps in the literature and motivate us to explain the breakdown in transition structure at high energy. Armed with the most previous finding, we study the boundaries of several nonreactive droplets appeared on the DS coincide with the emergence of additional PODSs. This is done in Chapter 4 by evaluating an ode solver used along with this research in order to meet our primary goals and purpose. This ode solver is stored on Matlab and tested among others based on an invariant property which is the cornerstone of any dynamical study. We build on the previous findings on both symmetric sides of the SSPO and make sure the methods used are sufficient. This kind of study raised some questions corresponding to how the dynamic transit regular behaviour to chaotic in a system known to be regular at low energy. In Chapter 5, we shed light to chaotic scattering, recrossing issues and those invariant manifolds connected to the periodic orbit cause the bifurcation in the transition state structure. This includes the trajectories behaviour near the stable manifolds of the UPO and the boundary between those cross the DS and those reflected back is investigated. In addition to recrossing phenomena is studied on PSS located at the DS for different energy values regime. Finally, we demonstrate the stable and unstable manifold belong to the UPO in order to show their heteroclinic intersections.

Chapter 2

Theoretical Background

2.1 Introduction

Transition State Theory (TST) [1, 22–26, 30] appears in many aspects of applications such as cosmology [45], atomic physics [46, 47], celestial mechanics [48], solid diffusion jumps [49] and cluster rearrangements[50]. However, TST plays an important role in the chemical reaction rate theory in particular to determine the rate of the collinear hydrogen exchange chemical reaction. The rate is calculated based on computing the total flux of trajectories directed from reactant to product regions. These regions are assumed to be separated by a surface calling "Dividing Surface". The Dividing Surface (DS) is assumed to be a surface of no return (trajectories that have already passed through from reactant to product regions will not recross it back).

Transition state theory provides a simple approximation to the reaction rate based on those trajectories passing through the dividing surface. The fundamental assumption for the TST guarantees the rate to be exact if and only if no trajectory crosses the DS more than once. However, classical mechanics in nature may yield recrossing effect, which is a common reason leading to TST failure. Because recrossing violates the fundamental assumption of TST, the projection of the SSPO solved the problem in configuration space. Generalising the concept of the symmetric stretch (DS) in phase space taken by

many authors solved the recrossing problem for a range of energies up to the bifurcation threshold. However, above the first bifurcation energy, nonreactive trajectories invalidate the TST calculation at higher energies. The new VTST approaches [29] consider all possible dividing surfaces of which only one surface is preferred with minimum flux. So the TST would provide an upper bound to the rate.

Above the energy barrier, the optimal dividing surface works like a bottleneck through which only reactive trajectories can pass during a reaction. Hence, the nonreactive trajectories do not cross it at all. As the energy increases, the bottleneck becomes wider and nonreactive trajectories may recross the DS in their way back so one can construct the DS at the saddle point. The bottleneck characterising the so-called " Transition State" or " activated complex"is not just a point. Thus, what we need is a periodic orbit serves as the DS.

The notion of Transition State (TS) is the cornerstone of the TST which can be traced back to stand out in the work of Marcelin [25] and more precise by Eyring–Polanyi [26] and Wigner [51] in their treatment to calculate the absolute reaction rate of the collinear hydrogen exchange. Their remarkable work is the culmination of experimental and theoretical investigations on a potential energy surface so that the TS is supposed to be at the saddle point barrier. In the configuration space, they defined the TS as the steepest ascent path from the barrier that connects two separated valleys associated with reactants and products regions. Their contributions had survived criticism over recrossing and provide a simple way to formulate the reaction rate. Pechukas *et al* [21, 52] found the exact TST up to about 0.1 eV. One year later, Miller *et al* [53] discussed whether the DS constructed in configuration space such that the TST becomes valid at low energy. Their work provided an overview of the reaction rate within the reaction region for both the collinear and three-dimensional configurations. Their calculations neglected numerical error of the quantum effect, which led to the shortcoming at the higher energy. Later developments were made by Evans, Farkas, Pelzer explained for example in Ref [24, 54].

In phase space, a single periodic orbit serves as a DS with no return at a range of low energies above the reaction threshold. As the energy increases, the collinear system

accepts several periodic orbits undergone series of bifurcations led to complicated dynamics structuring recrossing dividing surfaces. These DSs lead to the variational TST approach that investigates all involved periodic orbits and selects one from all possible Periodic Orbits Dividing Surfaces(PODSs) as the dividing surface with minimum flux. However, recrossing the PODS with small flux shed light back to reaction rate calculation and the DS breakdown. Puchukas and Pollak [29, 30, 55] realised that if a periodic orbit projected into configuration space, it would have stationary flux and would solve the problem of the VTST in a system with two degrees of freedom. The VTST principle is remarkable and considerable only in configuration space which differs from the phase space described in section 2.5. New formation to the VTST in phase space is essential, and there is a chance to find a periodic orbit with zero derivatives to solve the problem and extend the work. High computing process is essential, while an advance theory encourages scientists to address the real dynamical system.

Until the 1970s, theoretical understanding and numerical investigations helped to improve the problem beyond configuration space. Such development combined with vital tools such as Poincaré surface of section shed light back to the dynamics of a reactive system. This kind of progress can be seen in the work of Mackay, Perival and Meiss [27, 28] who were interested in finding a space barrier in survival torus' neighbourhood.

In the 1980s, the idea of invariant manifolds was used in studying several reactive systems by Davis *et al* [34, 56, 57]. From the nonlinear dynamics, such as manifolds, attached to PODS, divide phase space into different regions. In addition to that, Jaffé and Tiyapen [58–60] developed this to form unimolecular complexes in order to describe the structure of invariant fractal in phase space. Even though such new techniques are applied to the system with two degrees of freedom, it is only concerned for classical TST when single PODS partitions the phase space. This effort should extend a study of reactive systems when multiple PODSs.

Recently, the normal form utilised to study the neighbourhood of the TS for the many-body problem by Komatsuzaki et al [61–64]. The use of Lie transformation helps to construct the DS for many dynamical systems. Even though, Li *et al* [43] have studied the $H + H_2$ reaction with three degrees of freedom using the so-called partial normal

form, the problem in two degrees of freedom is still an active topic where the change in the structure of the DS is not understood yet. Moreover, Allahem *et al* [38] have computed the centre manifold of the saddle point to understanding the dynamics leading to recrossing DS for the collinear hydrogen exchange reaction. Their efforts are extended similarly but far away from the SSPO to figure out a phase space object responsible for the recrossing problem at a specific (high) energy.

Knowledge of the recent work done by Allahem [41] helps us to test his hypothesis of the existence of the phase space object that is carefully responsible for the shortcoming of TST in the four-dimensional system. In comparison, Allahem's work agreed with others such as Iñarrea *et al* [20] who have found the TST breaks down at about 0.2 e.V. above the potential energy barrier. Their finding that the TST is exact up to equivalent energy to ours at $E \approx -4.14676$ e.V. Whereas, the DS is filled up with reactive island only down that energy value at which the saddle-node bifurcation takes first place.

It knows that the first nonreactive trajectories begin to occur in the DS at the first bifurcation of the saddle-node type explained in Chapter 3.5.1. In the collinear case, stable and unstable periodic orbits are created on both sides of the saddle point [20, 41, 43]. Recently, Allahem has assumed that nonreactive trajectories are separated from reactive trajectories by invariant manifolds associated with the Unstable Periodic Orbit (UPO). He was able to consider the stable manifolds of the UPO which intersects the DS on the boundary of the main nonreactive layer (namely stable intersection due to him). Nevertheless, to find such an invariant manifold, he used the linear approximation that is broken far away from the UPO. This leads us to an interesting question to discuss in the thesis is: What is the boundary between reactive and nonreactive trajectories at specific high energy?

In what follows, a brief overview is given in section 2.2 about the definition of the Hamiltonian system and the TST rate formation given in section 2.3. After that, we give general formations to the phase space where the structure of the dividing surface is explained as well as the NHIM construction in phase space. These geometrical structures associated to a class of linear Hamiltonian systems close to a saddle point represented in section 2.4. We move over to describe the structure of the transition state in phase

space differed from the configuration space. That will follow by introducing the stability of periodic orbit in general.

2.2 Hamiltonian Dynamical System

Goldstein [65] and Wiggins [66] provide a good portion of the literature review in Hamiltonian vector field. We shall give a brief definition to the Hamiltonian system that describes such dynamical behaviour of the flow.

Let $H(q,p)$ be a smooth real valued function of generalised coordinates q_i's and their conjugate momenta p_i's. The Hamiltonian system is of the form

$$\dot{q_i} = \frac{\partial H}{\partial p_i} \qquad \dot{p_i} = -\frac{\partial H}{\partial q_i}, \tag{2.1}$$

for $i = 1, 2, ..., n$ where $\dot{q_i}$ and $\dot{p_i}$ represent the equations of motion and H is the Hamiltonian function. In fact, these equation are derived from the second Newton's Law in which the forces are potential function ($F = -\nabla V$). This can be rewritten in the Vector Space notation as

$$\dot{x} = J \cdot \nabla H, \tag{2.2}$$

where

$$J = \begin{bmatrix} 0_n & I_n \\ -I_n & 0_n \end{bmatrix},$$

is the $2n$ Poisson matrix and

$$\nabla H = (\frac{\partial H}{\partial q_i}, \ldots, \frac{\partial H}{\partial q_n}, \frac{\partial H}{\partial p_i}, \ldots \frac{\partial H}{\partial p_n}).$$

In many mechanical system H represents the total energy of the system and

$$H(q,p) = T(q,p) + V(q),$$

where T represents the kinetic energy and $V(q)$ is the potential energy. Note that, if the Hamiltonian H does not depend on time t explicitly, then the total energy is constant.

By (2.1),

$$\frac{d}{dt}H(q(t),p(t)) = \frac{\partial H}{\partial q}\frac{dq}{dt} + \frac{\partial H}{\partial p}\frac{dp}{dt} = 0,$$

Hence $H(q(t),p(t)) = H(q(0),p(0)) = E$ which is called the conservation of energy. However, if the Hamiltonian $H(q,p,t)$ depend on time t, then the total energy is not conserved.

Hamiltonian principle

A particle in phase space takes the true path $(q(t),p(t))$, $t \in [t_0,t_1]$ which is a solution to the Hamilton's equations (2.1), if and only if it is an extremum of the functional:

$$\delta \int_{t_0}^{t_1} \sum_{i=1}^{n} p_i dq_i - H(q(t),p(t))dt,$$

where the integrant is vanish only when the initial and final points of the boundary conditions is fixed such that

$$\big(\delta q(t_0), \delta p(t_0)\big) = \big(\delta q(t_1), \delta p(t_1)\big).$$

2.2.1 Symplectic transformation

A symplectic (canonical) transformation transfers the old Hamiltonian $H(q,p,t)$ to a new Hamiltonian $K(Q,P,t)$ by changing the old conjugate coordinates q and momenta p to a new conjugate coordinates Q and new momenta P in phase space which satisfy Hamilton's equations of motion (2.1) .

However, if the system does not depend explicitly on time t, then the old Hamiltonian is going to be the same as the new one because any region evolved in time preserves its area.

2.2.2 Symplectic Forms

A symplectic vector space is parallel to the vector space which is tangent to the path in phase space. This space is equipped with a symplectic form that can be defined by the standard inner product $\langle \cdot, \cdot \rangle$ on the phase space $\mathbb{R}^{2n}$ as follows

$$\Omega(u, v) \equiv \langle u, Jv \rangle, \qquad u, v \in \mathbb{R}^{2n}. \tag{2.3}$$

The Hamilton's equations of motion can be derived from the symplectic structure $\Omega(\cdot, \cdot)$ using the following formula

$$\Omega(X_H(x), v) = \langle DH(x), v \rangle, \qquad x = (q, p) \in \mathbb{R}^{2n}, v \in \mathbb{R}^{2n}. \tag{2.4}$$

Assume $X = (\dot{q}, \dot{p})$ be an arbitrary vector field on the $\mathbb{R}^{2n}$ phase space and $DH = (\frac{\partial H}{\partial q}, \frac{\partial H}{\partial p})$. Therefore, the equation (2.4) becomes

$$\Omega((\dot{q}, \dot{p}), v) = \langle \left(\frac{\partial H}{\partial q}, \frac{\partial H}{\partial p} \right), v \rangle.$$

Thus, using the inner products

$$\begin{aligned} L.H.S = \langle (\dot{q}, \dot{p}), Jv \rangle = \langle -J(\dot{q}, \dot{p}), v \rangle &= \langle \left(\frac{\partial H}{\partial q}, \frac{\partial H}{\partial p} \right), v \rangle, \quad \text{because } J^T = -J, \\ \langle (-\dot{p}, \dot{q}), v \rangle &= \langle \left(\frac{\partial H}{\partial q}, \frac{\partial H}{\partial p} \right), v \rangle. \end{aligned}$$

For fixed $v \in \mathbb{R}^{2n}$,

$$\langle (-\dot{p}, \dot{q}) - \left(\frac{\partial H}{\partial q}, \frac{\partial H}{\partial p} \right), v \rangle = 0.$$

Hence,

$$(-\dot{p}, \dot{q}) = \left(\frac{\partial H}{\partial q}, \frac{\partial H}{\partial p} \right),$$

which gives the Hamilton's equations in (2.1).

2.2.3 Eigenvalues of Symplectic Matrices

Assume the symplectic (canonical) transformation transformed the old Hamiltonian to the new Hamiltonian (say g) as

$$g : (q, p) \mapsto (Q(q, p), P(q, p)).$$

The Jacobian of g can be written as

$$A = \begin{pmatrix} \frac{\partial Q}{\partial q} & \frac{\partial Q}{\partial p} \\ \frac{\partial P}{\partial q} & \frac{\partial P}{\partial p} \end{pmatrix}, \tag{2.5}$$

which is a $2n \times 2n$ matrix (A). Let multiply this with the matrix (2.2) to get

$$A^T J A = J, \quad (JA)^T = JA \quad \text{and} \quad A^{-1} = J^{-1} A^T J,$$

which is the condition of the so-called symplectic matrix. Also, the Poisson matrix J satisfies

$$J^{-1} = J^T = -J \quad \text{and} \quad J^2 = -I_{2n}.$$

The eigenvalues of the symplectic matrix (A) can be found by solving the roots of the characteristic polynomial

$$poly(\lambda) \quad = \quad \det(A - \lambda I_{2n}),$$

The following proposition determines how the eigenvalues of the symplectic matrices will look like

Proposition 2.1. ***Wiggins*** *[66] Let A to be a symplectic matrix and $\lambda \in \mathbb{C}$ be an eigenvalue of A. Then λ^{-1}, $\bar{\lambda}$ and $\bar{\lambda}^{-1}$ are also eigenvalues of A. If λ is an eigenvalue of multiplicity k, then λ^{-1} is an eigenvalue of multiplicity k too. Also, the multiplicities of the eigenvalues $+1$ and -1, if they occur, are even.*

If the symplectic matrix A has real entries, then the eigenvalues of A will have the following properties: if λ is a real eigenvalue then the inverse eigenvalue λ^{-1} is also real.

Moreover, if λ is a complex eigenvalue, then the conjugate $\bar{\lambda}$ is also a complex eigenvalue. Therefore, if $\lambda = 1$ or $\lambda = -1$, then they must be repeated eigenvalues.

Note that the Poisson matrix represented the Hamiltonian system fixes one eigenvalue to 1, and thus, the other eigenvalue is given by the symplectic condition to be equal to one. Therefore, the remaining $2n - 2$ eigenvalues need to calculate in order to see the type of stability of n degrees of freedom Hamiltonian system.

2.3 Transition State Theory Rate

Transition state theory (TST) provides a good approximation to the rate of a chemical reaction. The more reactive trajectories leave the transition state through the dividing surface to the product side than those recross it leads to a more accurate rate. Because the reaction rate can be overestimated if some trajectories return back to the reactant side and encountered as reactive trajectories. This problem can be solved by choosing a dividing surface of minimum flux with respect to the transition state's location. Therefore, the TST will provide an upper bound to the reaction rate because the TST includes reactive events to the flux integral and exclude those trajectories with a negative contribution. The following integral gives the flux through the dividing surface for computing the exact rate in phase space

$$K_{\text{exact}} = \int ds(\mathbf{p}/m)\delta(E - H(q,p))\chi_a(q,p), \tag{2.6}$$

where the characteristic function of the reactive trajectory is given by

$$\chi_a = \begin{cases} 1 & \text{reactive trajectory} \\ 0 & \text{otherwise} \end{cases}$$

and $\delta(E - H(q,p))$ is the density function of phase point such that E is fixed energy. $H(q,p)$ is assumed to be the total energy of the system. $\mathbf{p}/m$ is the velocity motion of the trajectories. In fact, following all trajectories in order to compute the exact rate is a difficult task compared with the TST rate. For the TST rate, it is easy to distinguish

whether the trajectory is reactive or not by looking at the sign of the momentum in the initial condition. This idea gives an approximation to the rate by the characteristic function

$$\chi_b = \begin{cases} 1 & p > 0 \\ 0 & \text{otherwise} \end{cases}$$

and as a result, the flux integral in (2.6) can be written as

$$K_{TST} = \int ds(p/m)\delta(E - H(q,p))\chi_b(q,p). \tag{2.7}$$

So, if $\chi_b = \chi_a$, then the TST rate is exact and the determined dividing surface is recrossing–free [29].

The choice of a dividing surface plays an important role in estimating the TST rate, which is strictly based on the recrossing–free assumption. If a dividing surface has been chosen, for example, in the reactant side, then most trajectories would have enough energy to recross the surface as soon as they are reflected by the barrier, then many recrossing would be noted. Also, the direction of a reaction can affect the approximated rate if a dividing surface was located in the intersection area; some reactive trajectories cross the dividing surface from the opposite side. As a result, these recrossing should be denoted with a different sign in the flux integral [36]. In fact, many recrossing will be noted in most dividing surfaces which lead to a loss in the accuracy of the reaction rate. This problem is explained in Chapter 5.9.

2.4 Phase Space Geometrical Structure close to the saddle point

In this section, the theory of phase space enables us to develop the structure of n dof linear Hamiltonian system that is appropriate for reaction dynamics' study [36]. We will show some phase space objects in order to describe the transition dynamics, including the energy surface, the normally Invariant Manifold (NHIM) which is a higher-dimensional object of a saddle [35] (the symmetric stretch associated with its stable and unstable

manifolds in collinear system) and the dividing surface that can be constructed by using the symmetric stretch periodic orbit contains the saddle point [21].

The problem we may face regarding the dividing surface in phase space is that dividing surface is defined originally in configuration space and proper treatment has to be extended to phase space. The recrossing free DS in phase space is not projected to that analogue DS in the configuration space. Investigation for understanding the structure of the phase space is based on the definition of the TST in the configuration space.

Recently, Uzer *at al* [36] and Komatsuzaki *et al* [62] have shown that the dividing surface can be constructed in phase space for both non/linear Hamiltonian systems in multi-degrees of freedom. A normally hyperbolic invariant manifold (NHIM) replaces the periodic orbit dividing surface (PODS) in a system of many degrees of freedom. Most the essential formation is regarding the NHIM, its stable and unstable manifolds because the DS can be constructed with recrossing free trajectories in the area close to the NHIM. This area can be determined by the symmetric stretch periodic orbit in two dof.

2.4.1 The Hamiltonian with n degrees of freedom

Now we will present the structure of n dof for linear Hamiltonian system near centre $\times$ centre $\times ... \times$ saddle of rank one [36]. Not only is useful when we are concerned with the behaviour of the linear dynamic state near a stationary point, but also for the further study of the nonlinear system. Consider the following Hamiltonian of the quadratic form

$$H = \frac{1}{2}\Big(\sum_{j=1}^{n} p_j^2 + \sum_{j=1}^{n-1} \omega_j^2 q_j^2 - \lambda^2 q_n^2\Big), \tag{2.8}$$

where $(q_j, p_j) \in R^{2n}$ and the Hamiltonian system is given by

$$\begin{aligned} \dot{q_j} = \tfrac{\partial H}{\partial p_j} = p_j, \quad \dot{p_j} = -\tfrac{\partial H}{\partial q_j} = -\omega_j^2 q_j \\ \text{where} \qquad\qquad j = 1, ..., n-1 \\ \dot{q_n} = \tfrac{\partial H}{\partial p_n} = p_n, \quad \dot{p_n} = -\tfrac{\partial H}{\partial q_n} = \lambda^2 q_n. \end{aligned} \tag{2.9}$$

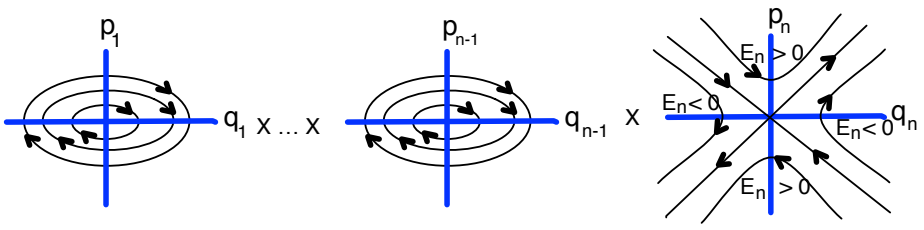

FIGURE 2.1: *Phase portrait for the uncoupled systems. Adapted from that taken from [36]*

This system contains of $n-1$ uncoupled linear oscillators, with the remaining dof representing a parabolic barrier. Thus (q_n, p_n) are referred to the reaction coordinates while the remaining coordinates showing the bath coordinates.

The phase portrait of n uncoupled systems are shown in Figure 2.1. It can be seen those trajectories go from $q_n > 0$ to $q_n < 0$ (or vice versa) are undergo reaction. This figure shows that there are two types of reactive trajectories ($E_n > 0$). Those trajectories with $p_n > 0$ are called forward reactive trajectories which cross the DS in their future evolution. The second type is the backward reactive trajectories with $p_n < 0$ which do cross the DS in their past evolution. Note that nonreactive trajectories ($E_n < 0$) do not have enough energy to cross the DS as shown in Figure 2.1.

In phase space , the stability matrix evaluate the eigenvalues at the stationary point of the flow is different from that used in the configuration space due to momenta. These eigenvalues can be evaluated by the matrix at the stationary point as follow:

$$\begin{pmatrix} \frac{\partial \dot{q}}{\partial q} & \frac{\partial \dot{q}}{\partial p} \\ \frac{\partial \dot{q}}{\partial p} & \frac{\partial \dot{q}}{\partial p} \end{pmatrix} = \begin{pmatrix} \frac{\partial^2 H}{\partial q \partial p} & \frac{\partial^2 H}{\partial^2 p} \\ -\frac{\partial^2 H}{\partial^2 q} & -\frac{\partial^2 H}{\partial q \partial p} \end{pmatrix}. \tag{2.10}$$

There are n pairs of eigenvalues which are either complex numbers with their conjugates or real numbers with their inverses. The complex eigenvalues respond to a stable degree of freedom while the real eigenvalues represent unstable degrees of freedom [54]. Readers are referred to [67] for more details regarding when the eigenvalues are equal to zero, which is a rare case.

The Hamiltonian system of $n-1$ uncoupled equations has a stationary point at $p_j = q_j = 0$ at the zero energy. The linearisation around the saddle point gives the eigenvalues $\pm\lambda$ to describe the hyperbolic direction and the complex eigenvalues $\pm i\,\omega_j$ which describe the elliptic directions of the saddle point.

2.4.2 The energy surface

At fixed energy $h > 0$ above the reaction threshold, the dynamic occurs on $(2n-1)$ dimensional energy surface defined by

$$\frac{1}{2}\sum_{j=1}^{n} p_j^2 + \frac{1}{2}\sum_{j=1}^{n-1}\omega_j^2 q_j^2 - \frac{\lambda^2}{2}q_n^2 = \text{constant} = h > 0. \tag{2.11}$$

One can split the energy to describe each degrees of freedom seperately as follows

Assume that $h > 0$, $\omega_j > 0$ for $j = 1, \ldots, n-1$ and $\lambda > 0$.

$$\begin{aligned} &\frac{1}{2}(p_j^2 + \omega_j^2 q_j^2) = E_j \qquad \text{for } j = 1, \ldots, n-1, \\ &\frac{1}{2}(p_n^2 - \lambda^2 q_n^2) = E_n, \end{aligned} \tag{2.12}$$

where $E_1 + E_2 + \cdots + E_n = h$.

For fixed q_n, the geometry of energy surface can be seen through the section as a $(2n-2)$ sphere with radius $\sqrt{\frac{\lambda^2}{2}q_n^2 + h}$ if we rewrite the (2.11) as follows

$$\frac{1}{2}\sum_{j=1}^{n} p_j^2 + \frac{1}{2}\sum_{j=1}^{n-1}\omega_j^2 q_j^2 = \frac{\lambda^2}{2}q_n^2 + h. \tag{2.13}$$

Thus, we can see the energy surface as a hyper-cylinder $S^{2n-2} \times \mathbb{R}$.

2.4.3 The NHIM

Note that if we set $p_n = q_n = 0$ in (2.9), then $\dot{p}_n = \dot{q}_n = 0$. As a result, $p_n = q_n = 0$ is an invariant manifold, namely the centre manifold of the saddle point (i.e. If you start in you stay in for all time). This invariant manifold is of $(2n-2)$ dimension which intersects with the energy surface such that for a fixed energy $h > 0$

$$\frac{1}{2}\sum_{j=1}^{n-1} p_j^2 + \frac{1}{2}\sum_{j=1}^{n-1} \omega_j^2 q_j^2 = h;$$

$$p_n = q_n = 0. \tag{2.14}$$

is a $(2n-3)$ dimensional sphere $\left(S_h^{2n-3}\right)$. This is an example for the NHIM that forms the bottleneck in phase space (called later the central sphere). The NHIM is a hypersphere which means the dynamical expansion and contraction rate transverse to the sphere are larger in directions than those tangent to it. This is clear since the dynamics to the sphere are normal similar to that described in the $q_n - p_n$ portrait correspond to the saddle and thus the NHIM ($(2n-3)$ sphere) has stable and unstable manifolds attached to it. These manifolds are of $(2n-2)$ dimension and denoted by $W^s(S_h^{2n-3})$ and $W^u(S_h^{2n-3})$, respectively. Since these manifolds are of one less dimension than the energy surface, they are separaticies by which reactive and nonreactive trajectories divided in phase space. These manifolds are known to separate reactive from nonreactive trajectories in phase space. The stable and unstable manifolds guide the system from the reactant configuration towards the DS and into the product region.

The un/stable manifolds are given by

$$W^u(S_h^{2n-3}) = \{(q_1, ..., q_n, p_1, ..., p_n) \mid \frac{1}{2}\sum_{j=1}^{n-1} p_j^2 + \frac{1}{2}\sum_{j=1}^{n-1} \omega_j^2 q_j^2 = h,\ p_n = \lambda q_n\}, \tag{2.15}$$

$$W^s(S_h^{2n-3}) = \{(q_1, ..., q_n, p_1, ..., p_n) \mid \frac{1}{2}\sum_{j=1}^{n-1} p_j^2 + \frac{1}{2}\sum_{j=1}^{n-1} \omega_j^2 q_j^2 = h,\ p_n = -\lambda q_n\}.$$

Clearly, the un/stable manifolds of the NHIM have the geometry of spherical cylinders

($S^{2n-3} \times \mathbb{R}$) which are referred to as the reaction cylinders. Since they are of one dimension less than the NHIM, they will acts as boundaries between reactive and nonreactive trajectories because the unstable and stable manifolds of the NHIM have the same energy as the two lines $p_n = \lambda q_n$ and $q_n = -\lambda p_n$ attached to the saddle. However, if $p_n > 0$, then un/stable cylinders are referred to the forward reactions. Similarly for $p_n < 0$ that is related to the backward reactions cylinders. These two kinds of reactions in the stable and unstable cylinders are defined by the following.

The stable forward cylinder is

$$W_f^s(S_h^{2n-3}) = \{(q_1, ..., q_n, p_1, ..., p_n) | \frac{1}{2}\sum_{j=1}^{n-1} p_j^2 + \frac{1}{2}\sum_{j=1}^{n-1} \omega_j^2 q_j^2 = h, p_n = -\lambda q_n > 0\}.$$

The stable backward cylinders

$$W_b^s(S_h^{2n-3}) = \{(q_1, ..., q_n, p_1, ..., p_n) | \frac{1}{2}\sum_{j=1}^{n-1} p_j^2 + \frac{1}{2}\sum_{j=1}^{n-1} \omega_j^2 q_j^2 = h, p_n = -\lambda q_n < 0\}.$$

The unstable forward cylinder

$$W_f^u(S_h^{2n-3}) = \{(q_1, ..., q_n, p_1, ..., p_n) | \frac{1}{2}\sum_{j=1}^{n-1} p_j^2 + \frac{1}{2}\sum_{j=1}^{n-1} \omega_j^2 q_j^2 = h, p_n = \lambda q_n > 0\}.$$

The unstable backward cylinder

$$W_b^u(S_h^{2n-3}) = \{(q_1, ..., q_n, p_1, ..., p_n) | \frac{1}{2}\sum_{j=1}^{n-1} p_j^2 + \frac{1}{2}\sum_{j=1}^{n-1} \omega_j^2 q_j^2 = h, p_n = \lambda q_n < 0\}.$$

Note that one can verify easily that the stable and unstable manifolds of the saddle must have zero energy value (i.e. $h = 0$) from (2.12). There the origin is a saddle point for Hamiltonian system (2.9). It has $(2n-2)$ dimensional centre manifold ($p_n = q_n = 0$), a stable manifold of one dimension that is given by $q_j = p_j = 0, j = 1, ..., n-1, p_n = -\lambda q_n$, and unstable manifolds of the same dimension that is given by $q_j = p_j = 0, j = 1, ..., n-1, p_n = \lambda q_n$. The intersection of the centre manifolds of the origin with the energy surface defines the NHIM which can be bounded by the symmetric stretch in two degrees of freedom. Hence, the stable and unstable manifold of the NHIM belong to the

symmetric stretch periodic orbit used to construct the DS. The centre manifold of the origin contains a family of the SSPOs for each energy parameter h.

We move now to the construction of a dividing surface (DS).

2.4.4 The dividing surface (DS)

The dividing surface of recrossing–free property can be realised by setting $q_n = 0$. This dividing surface is of $(2n-2)$ dimensional sphere and defined by (2.4.3).The NHIM acts as an equator splitting the DS into two hemispheres $p_n > 0$ and $p_n < 0$. All trajectories, except those within the NHIM, pass once through the DS, undergo reaction (reactive). Those trajectories with $p_n > 0$, passing through the sphere are forward reactive. The backward reactive trajectories are of opposite p_n sign to the forward reactive. All trajectories with $p_n = 0$ within the NHIM will remain in the DS for all times.

By the language of dimensions, if there exist n degrees of freedom, there will be a $2n$ dimensional phase space. By fixing the energy h = constant, the phase space reduced to $(2n-1)$ energy surface and $(2n-2)$ for the centre manifold section. The NHIM is $(2n-3)$ dimensional sphere and has an unstable and stable manifold of $(2n-2)$ dimensions. However, for two degrees of freedom, the NHIM is an unstable periodic orbit in phase space. It is a three-dimensional sphere in three degrees of freedom.

In summary, the dividing surface will have several features. Firstly, it is a surface of no return in a linear Hamiltonian system. All reactive trajectories pass through the dividing surface once and only once. Secondly, in the $(2n-1)$ dimensional energy surface, the forward and backward dividing surfaces have the structure of $(2n-2)$ dimensional balls referred to $B_f^{2n-2}(h)$ and $B_b^{2n-2}(h)$, respectively . Finally, it is bounded by an invariant $(2n-3)$ dimensional sphere, the (NHIM).

In reaction rate's language, the flux through the dividing surface in the energy surface plays a crucial role in finding the reaction rate. This is the cornerstone of reaction dynamics.

Now, let's study the role of unstable spherical cylinders in determining the region of reactive trajectories.

2.4.5 Cylindrical Manifolds of Phase Space

Uzer et al [36] stated that *the un/stable spherical cylinders bound a region in the energy surface that is divided into two disconnected components by the dividing surface. All reactive trajectories start inside one connected component cross the dividing surface and leave the dividing surface into the other connected components.*

Rewrite the energy surface equation as

$$\frac{1}{2}\sum_{j=1}^{n-1}(p_j^2+\omega_j^2 q_j^2)+\frac{1}{2}(p_n+\lambda q_n)(p_n-\lambda q_n)=h. \tag{2.16}$$

The reactive trajectories satisfy

$$0<\frac{1}{2}p_j^2+\frac{1}{2}\omega_j^2 q_j^2=E_j<h, j=1,...,n-1,$$

$$\frac{1}{2}(p_n+\lambda q_n)(p_n-\lambda q_n)=E_n>0, \tag{2.17}$$

such that

$$\sum_{j=1}^{n}E_j=h.$$

So, from the equality (2.17) $E_n>0$ if and only if

$$(p_n+\lambda q_n)>0,\ (p_n-\lambda q_n)>0\ \ (i.e.\ p_n>0, (\text{forward reactive area }) \tag{2.18}$$

or

$$(p_n+\lambda q_n)<0,\ (p_n-\lambda q_n)<0\ \ (i.e.\ p_n<0, (\text{backward reactive area}) . \tag{2.19}$$

Equation (2.18) defines the boundary of the forward reactive area such that

$$p_n = \lambda q_n, \qquad p_n = -\lambda q_n, \qquad p_n > 0,$$

that is $W_f^u(S_h^{2n-3})$ and $W_f^s(S_h^{2n-3})$. Similarly for the boundary of the backward reactive area given by

$$p_n = \lambda q_n, \qquad p_n = -\lambda q_n, \qquad p_n < 0,$$

which is $W_b^u(S_h^{2n-3})$ and $W_b^s(S_h^{2n-3})$.

So far, we know that all reactive trajectories must pass through the TS ($q_n = 0$) and also, the forward reactive trajectories lie on the bounded region by $W_f^u(S_h^{2n-3})$ and $W_f^s(S_h^{2n-3})$. Similarly for the backward reactive trajectories with $E_n > 0$ that lie on the region bounded by the backward un/stable cylinders $W_b^u(S_h^{2n-3})$ and $W_b^s(S_h^{2n-3})$ that have been already explained.

Now, we will describe the reactive trajectories already in the reactant and product regions.

Consider the initial condition of the forward reactive trajectories with $p_n > 0$ and $q_n < 0$, which referred to as reactant segment. The trajectory has been shown in Figure 2.2 as a dashed curve and decaying in time until the q_n reaches zero, where is the location of the TS. Then, the trajectory is grown in the time when q_n increased to be positive. The product segment of trajectory is within $q_n > 0$ (shown in Figure 2.2).

For energy ($E_{tot} > E_{sp}$), the reactive trajectories take place and pass through the dividing surface. These trajectories will never return back at an energy above the threshold up to E_{tot^*}. Therefore, a family of cylinders will exist for $E_{sp} < E_{tot} < E_{tot^*}$. Similarly, for motion from products to reactants, a family of cylinders will exist. However, non-reactive trajectories will stay in either reactants or products side laying on cylindrical manifolds.

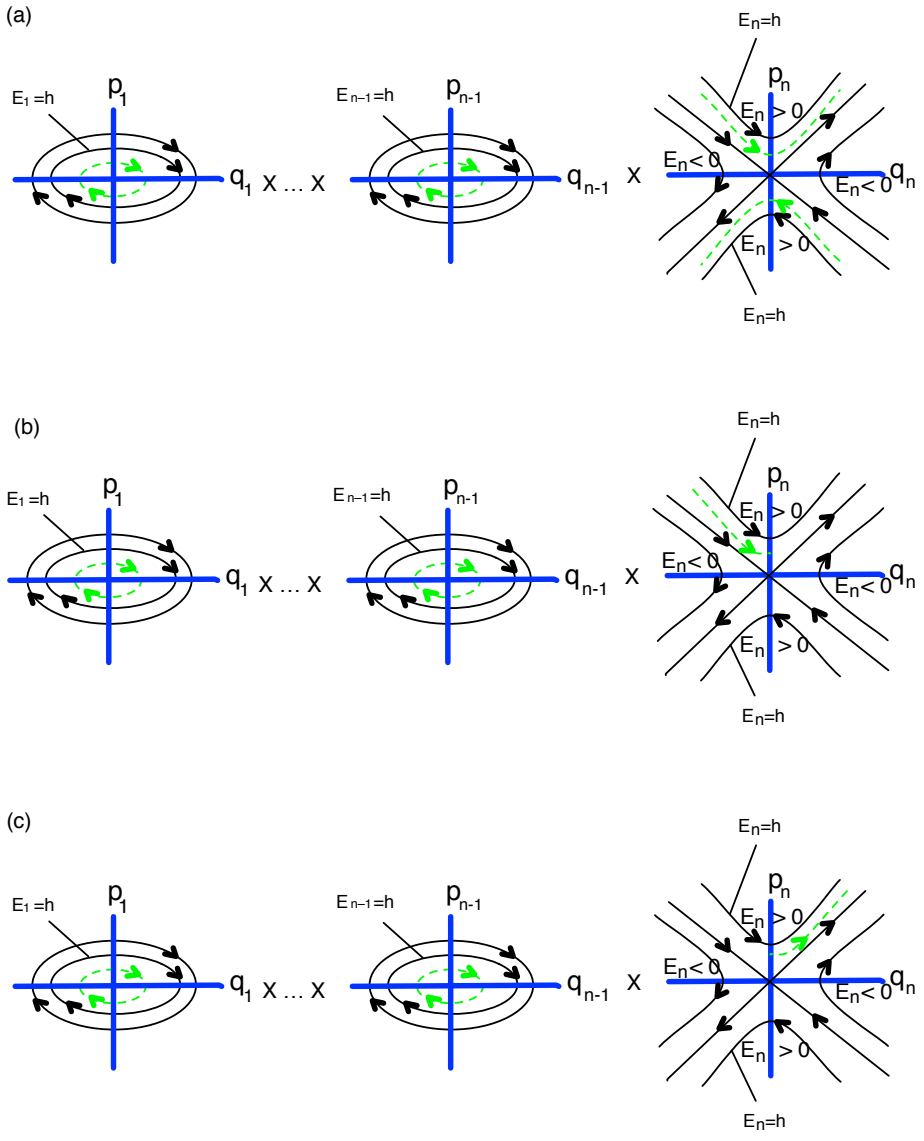

FIGURE 2.2: *(a) forward reactive in a dashed curves. (b) The reactants segment of the forward reactive trajectory.(c) The product segment of the forward reactive trajectory. Adopted from that in [36]*

2.5 Phase and Configuration Space

In this section, we declare why the phase space is highly needed as a generalisation space to the configuration space with some pros and cons. In chemistry literature, the transition state (TS) notion brings such confusion in terms of terminology. TS sometimes refers to the DS and on other times means the periodic orbit which is an invariant set contained in the DS. This confusion leads us to be more precise about the space where a trajectory crosses the DS.

In terms of dimensionality, the configuration space, where the potential energy surface is defined, is n dimensions while the total energy is only defined in $2n$ dimensional phase space. The DS is a phase space object which cannot be defined in configuration space because the unstable periodic orbit (PODS) in phase space is used to construct the DS and solves (locally) the recrossing problem in configuration space for 2 dof [21]. The intersection is only understood in configuration space where the periodic orbit is projected as a line segment. In addition to that, the invariant manifolds associated with the unstable periodic orbit which provide a qualitative description of the dynamics can only exist in phase space.

PES is the basis for understanding the structure of molecules associated with the dynamics well beyond stationary points and barriers. In configuration space, that surface represents only the position of the system while the minima are called potential wells. Between these minima, saddle points may exist. So, the molecule has to pass over the saddle in order to be transformed from one well to another. Therefore, these useful assumptions can be taken further in two steps. First, the Hamiltonian has to be in the form of kinetic energy function plus the potential. Secondly, the kinetic energy function contains only positive definite and quadratic momenta. Thus, the stationary point of the potential energy surface (configuration space) coincide with the stationary point of the total Hamiltonian in phase space. This only makes sense when the momenta are equal to zero, and the extremum of the potential energy is balanced at this point, e.g., in configuration space. These saddle points act as barriers in phase space and are being

ideal positions for the unstable periodic orbits. Their geometrical structure associated with the invariant manifolds will partition reactive from nonreactive regions.

The basic idea of VTST is that small flux is much better and we realise that PODSs have stationary flux (i.e. zero derivative means minimum flux). Pechukas and Pollak [21, 55] show that if a DS is an unstable periodic orbit projected in configuration space, it will have zero derivatives. Moreover, finding the stationary state and calculating the linear stability of such a system is not a difficult task in phase space. In configuration space, each point represents only the physical position of the system while in phase space, it represents a unique state.

2.6 Stability of Periodic Orbits

The stability or instability of periodic orbits of a Hamiltonian system describes the behaviour of the system near a periodic orbit. In particular, the behaviour of a non-periodic orbit is similar to a nearby stable periodic orbit as they evolve in time, while the system becomes in general chaotic in the neighbourhood of an unstable periodic orbit [41].

Consider the Hamiltonian system with $N+1$ degrees of freedom written in (2.2)

Now, we assume $x(t)$ is a periodic orbit with period T satisfying

$$x(t+T) = x(t).$$

Assume the deviation from the periodic orbit is

$$\bar{x} = x(t) + \xi(t),$$

where ξ is infinitesimally small. This is also a solution for the system (2.2) and then satisfying

$$\dot{x} + \dot{\xi} = f(x+\xi),$$

where f refers to the right hand side of (2.2). Using the Taylor expansion gives

$$\dot{x} + \dot{\xi} = f(x) + \frac{\partial f}{\partial x}\xi + ...$$

Then,

$$\dot{\xi} = \frac{\partial f}{\partial x}\xi,$$

where $\frac{\partial f}{\partial x} = \sum_k J_{ik}$ $\frac{\partial^2 H}{\partial x_k \partial x_j} = -(JP)_{ij}$,where P is the $Hessian$ matrix of the Hamiltonian (3.5) at the periodic orbit and ξ is the deviation from the periodic orbit in $(2N+2)$ dimensional phase space.

The linear stability of the periodic orbit with period $T > 0$ can be determined by solving the linearised system of the form

$$\begin{bmatrix} \dot{x} \\ \dot{\xi} \end{bmatrix} = \begin{bmatrix} f(x) \\ f_x\ \xi \end{bmatrix}; \begin{bmatrix} x(0) = x_0 \\ \xi(0) = I \end{bmatrix}, \tag{2.20}$$

where $f_x = J\ P$. Then integrating this until $t = T$ obtains the monodromy matrix A of the periodic orbit which satisfies the symplectic condition

$$A^T J A = J. \tag{2.21}$$

The eigenvalues of the monodromy matrix determine the stability type of the periodic orbit. These eigenvalues are called *multipliers* and obtained by finding the roots of the characteristic polynomial

$$Poly(\lambda) = \det(A - \lambda I_{2n}). \tag{2.22}$$

Since the matrix A is symplectic and its coefficients are real, if $\lambda \in \mathbb{C}$ is an eigenvalues of A, then $\frac{1}{\lambda}$ and their complex conjugates $\bar{\lambda}$, $\bar{\lambda}^{-1}$ are also eigenvalues for A [66].

Since the Hamiltonian system is conservative, then the symplectic condition will guarantee two eigenvalues to be equal to one. Therefore, the remaining $2n - 2$ eigenvalues need to be computed in order to determine the stability type of the periodic orbit.

Chapter 3

Hydrogen Exchange Reaction

3.1 Introduction

Since the 1930s, Transition State Theory (TST) has enhanced dynamical study in chemical reactions and provided a fundamental tool to compute the reaction rate. The benchmark reaction for the accuracy of the TST rate is the collinear hydrogen reaction

$$H_2 + H \rightarrow H + H_2.$$

There are several reasons for this, including the fact that it is frequently referred to as the most elementary reaction in the literature [68–72] and has three identical atoms, as well as the symmetry of the molecule. These hydrogen atoms are confined to move on a line and consist of three electrons and three protons. Due to its reaction simplicity, an accurate potential energy surface has been already calculated in the Born–Oppenheimer approximation [73]. The collinear hydrogen system is derived from a spatial system with three degrees of freedom (dof) involved vibration.

A molecule is originally a complex quantum system. The complexity of molecule structure has been investigated in the past few decades and open new areas of research in molecule physics[74]. Several techniques such as pulsed laser[75]–[76], hexapole state

selection [77], brute force methods[78]–[79] and hybrid are proposed to control molecule alignment and orientation [80]. The femtosecond two colour laser pulse was used to orient and align the CO molecule in the free–field space. The experiment shows that the physical mechanism can change the orientation of the molecule due to the rotational wave function. In 2014, Marcus *et al.* [81] declared in the parallel and crossed field configuration that it is possible to control the molecule alignment and orientation on the ultralong–range Rydberg molecules even in electric and magnetic fields. However, in the case of hydrogen, the coherence amplification technics to generate alignment and angular momentum orientation can be achieved by Stark control [82]. However, the collinear hydrogen atoms in our case are all confined to move on a straight line. Convention has been employed in many previous studies [39, 54] to circumvent the ensuing rotation, thus simplifying this. The phase space can be reduced to a plane where the collinear complex has not been affected by rotation around its axis.

We are mainly interested in studying the dynamics in the phase space for the collinear exchange reaction, known to be symmetric. This simple system, with two degrees of freedom, is an invariant in the sense that collinear configuration has not singularities in the phase space. The 2 dof system modelling the chemical reaction is most definitely the simplest imaginable one in the chemistry literature. Due to its simplicity, Born and Oppenheimer [73] calculated the potential energy surface, responding to atomics' position and their interaction potential.

For essential development regarding the potential energy surface, readers interested in quantum chemistry are referred to the literature in [68–72]. The Porter–Karplus potential energy function [13] has commonly been used as the standard potential function for the hydrogen exchange reaction in various dynamical studies and meet the purpose of this thesis. This function is explained and presented for the collinear configuration in section 3.2.

The potential energy combined with the kinetic energy is modelling the exchange of hydrogen reactions that can be expressed by the Hamiltonian function. The latter is known to govern the motion on the top of the barrier, where the potential energy approaches zero. In section 3.2, we discuss this configuration in more detail. This is

followed by the hydrogen exchange system which describes the equations of motion. After that, we are going to explain how to reduce the 3 dof full system to the collinear system, which the latter emphasise the case of study in the whole thesis. At the end of this chapter, known results combined with motivation are written to impress the purpose of the research.

3.2 Potential Energy Function

In this section, we introduce the potential energy function, which is effectively interacted with the collinear hydrogen atoms on a two-dimensional surface. We will then study the dynamics of the compound, responding to that interaction potential on configuration space.

The Porter–Karplus potential energy function [13] is given by:

$$V = (1/C_1)\left[-C_2 - (C_2^2 - C_1C_3)^{1/2}\right], \tag{3.1}$$

where

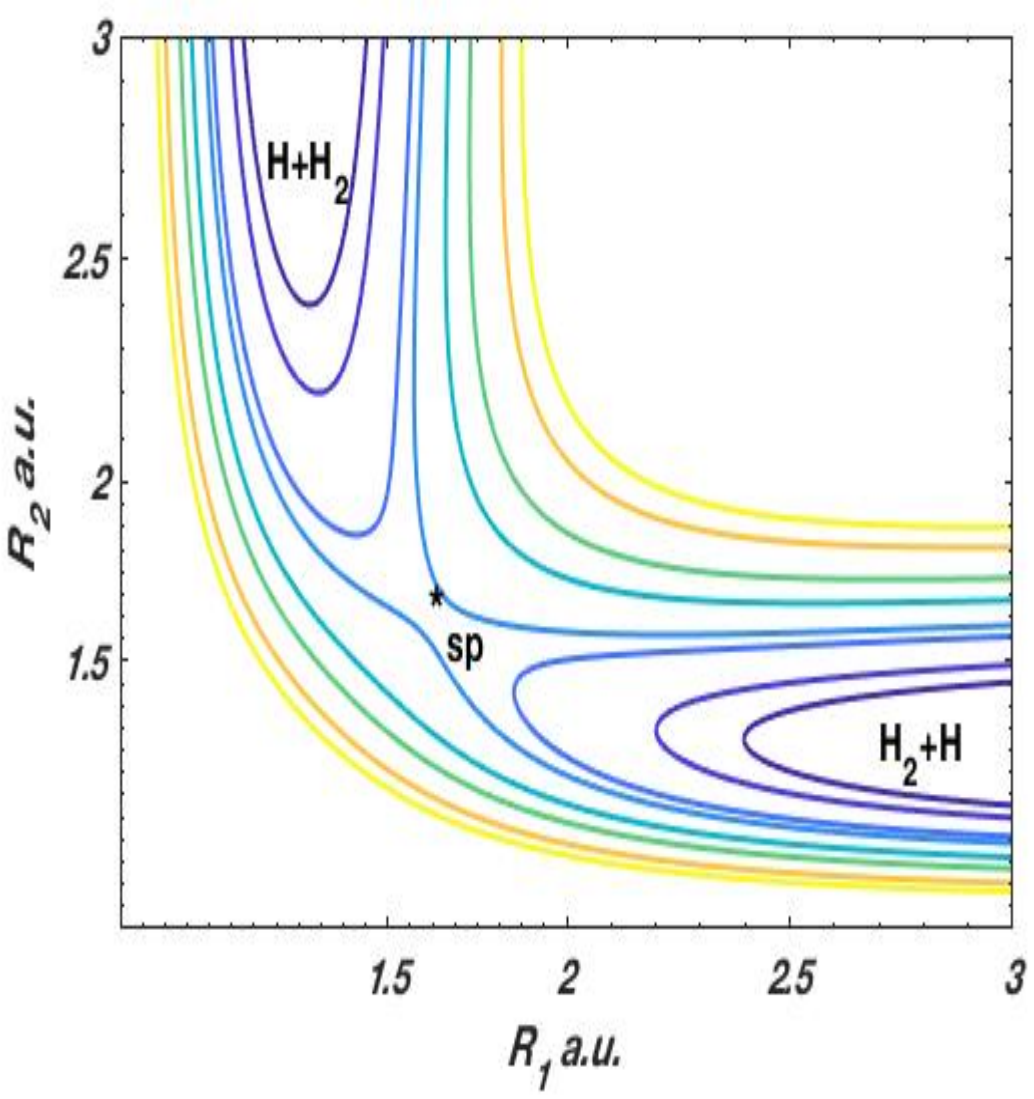

FIGURE 3.1: The potential surface for $H + H_2$ exchange reaction.

$$
\begin{aligned}
C_1 &= (1 - S_1S_2S_3)^2 - \frac{1}{2}\left[(S_1^2 - S_2^2)^2 + (S_2^2 - S_3^2)^2 + (S_1^2 - S_3^2)^2\right], \\
C_2 &= -(Q - J_{123})(1 - S_1S_2S_3) \\
&\quad + \frac{1}{2}[(J_1 - J_2)(S_1^2 - S_2^2) + (J_2 - J_3)(S_2^2 - S_3^2) + (J_1 - J_3)(S_1^2 - S_3^2)], \\
C_3 &= (Q - J_{123})^2 - \frac{1}{2}\left[(J_1 - J_2)^2 + (J_2 - J_3)^2 + (J_1 - J_3)^2\right], \\
Q &= Q_1^d + Q_2^d + Q_3^d, \\
Q_k^d &= \frac{1}{2}\left[{}^1E_k + {}^3E_k + S_k^2({}^1E_k - {}^3E_k)\right],
\end{aligned}
$$

TABLE 3.1: Parameters characterising the potential energy function. Taken from [13]

D_1 = 4.7466 e.V.	β = 28.2 e.V.
D_3 =1.9668 e.V.	ϵ = -17.5 e.V.
R_e =1.40083 a.u.	κ =0.60
α=1.04435 a.u.	λ =0.65
β =1.000122 a.u.	

where $k, l, m = 1, 2, 3$, with $m \neq l \neq k$. The potential energy expression depends on three variables, namely R_1, R_2, R_3 to describe distances between three atoms and contains nine parameters that are D_1, D_3, R_e, α, β, λ, κ, δ and ϵ. These parameters are outlined in Table 3.1. All energies are above the minimum energy barrier of the system, which is expressed in electron Volt (e.V.). Physical magnitudes like distances are given in atomic units (a.u.) as used in some previous work. These unit measurements will be used throughout this thesis.

The collinear chemical reaction is governed by three hydrogen atoms interacted on the potential energy surface (PES) presented in Figure 3.1. Two atoms form a molecule (R_1 is small) while one is at a distance and isolated (R_2 is large). The isolated one approaches the molecule, and there exists possibly a reaction of some sort, where the isolated atom then becomes part of the molecule (R_2 close enough). Once the molecule breaks a bond, one atom is naturally repelled (R_2 small and R_1 larger), as a result of the reaction. The potential energy surface will then not depend on R_1 in the new configuration. Similarly to that region where the isolated atom does not react, the potential describes atomic vibrational motion. These regions can be defined as before (reactants), and after (product) the reaction has taken place.

The concept of configuration space identifies different chemical regions on the PES to those represent reactants, and those identify products. These chemical features coincide with the PES that has two minima and a saddle point marked in Figure 3.1, which exists between the potential wells. The vicinity of the saddle attracts significant attention from those interested in transition dynamics, primarily because the saddle point is part

of the structure of transition, that coincides with the concept of the Transition State Theory. For instance, the Transition state (TS) is the steepest descent paths along with the decay in both directions on PES, defined by the eigenvectors associated with the saddle connecting the two minima, which are combined to identify the so-called reaction path. The joint structure termed the invariant manifolds, can only be recognised in phase space. Fortunately, the location of the saddle point at $R_1 = R_2 = 1.70083$ a.u. corresponding to the potential energy value of -4.3504 e.V. This coincides with those values found recently by Iñarrea *et al* [20] and earlier. The optimal DS can be allocated in this region where the reaction occurring coincides with the location of unstable periodic orbit around the saddle point.

Inarguably, the system must pass over that potential barrier only once per time, per reaction. During the reaction, those trajectories passing the DS are called reactive, otherwise nonreactive. The conventional TST identifies those reactive trajectories with one-time crossing during a reaction. However, the compound is symmetric collinear at the saddle point, and the PODS is the symmetric stretch periodic orbit that obeys the fundamental TST assumption for small energy intervals above the threshold, but suddenly collapses to act as the optimal DS once energy increases. The re-crossing issue is an apparent reason, in conjunction with the moving process of a trajectory that is governed by the kinetic energy explained in the next section.

3.3 Kinetic Energy

In this section, kinetic energy exerted from the motion of the hydrogen complex is explored.

The kinetic function is taken by Allahem [38], from that given by Waalkens *et al* [39], as follows:

$$T = \frac{1}{m_H}\left[p_r^2 + \frac{3}{4}p_R^2\right], \tag{3.2}$$

Where m_H is the mass of the hydrogen atoms that are connected by Jacobi coordinates, such that r and R are polar coordinates representing distances (shown in Figure 3.2).

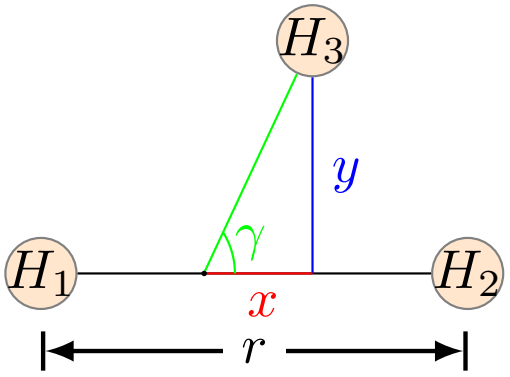

FIGURE 3.2: The coordinates for $H + H_2$ exchange reaction.

Under Cartesian transformation, the polar coordinates are transformed to those Cartesian coordinate in r, x, y shown in Figure 3.2 and the hydrogen kinetic energy function becomes in the form (3.2) as follows:

$$T = \frac{1}{m_H}\left[p_r^2 + \frac{3}{4}(p_x^2\right], \tag{3.3}$$

The shape of the complex can be described by three coordinates r, x, y representing distances between hydrogen atoms, as shown in Figure 3.2. These coordinates can be transformed (r, x, y) to $(r, x, -y)$ by a rotation around the horizontal axis. This is not of a subtle matter because not all configurations are similar. To avoid rotation, configuration with positive y and negative y are considered as different [38]. Restricting to the half-plane $(r, x, y \geq 0)$, the configuration space can be bounded by the collinear configuration with vanishing y at the x–axis where the system is reflected. Unfortunately, the collinear configuration is symmetric at the saddle point where the optimal DS is reasonably located. The Hamiltonian may be written as a sum of the kinetic and potential functions and their equations of motion form a full spatial system with three degrees of freedom given below.

3.4 The Exchange Hydrogen Hamiltonian System

The Hamiltonian system is obtained by identifying all configurations that are restricted to the half plane. These configurations express the full spatial system that can be explained with the help of Figure 3.2. We can define the three coordinates r, x, and y, where r describes the distance between H_1 and H_2, y represents the distance from H_3 to the bond H_1H_2, x is the displacement between the centre of mass of H_1 and H_2 and the intersection point with y at H_1H_2 bond. The triangular shape of the compound has R_1, R_2 and R_3 representing the distances between the atoms. Here, $R_1 = r$ and the other interatomic distances R_2 and R_3 are given by

$$R_2 = \sqrt{y^2 + (\frac{r}{2} + x)^2}$$

$$R_3 = \sqrt{y^2 + (\frac{r}{2} - x)^2}. \tag{3.4}$$

The (r, x, y) coordinates with their conjugate momenta spanned the phase space of vibrational motion [83, 84]. The Hamiltonian system of the hydrogen reaction is taken from Allahem *et al* [38] which is given by

$$H = \frac{1}{m_H}\left[p_r^2 + \frac{3}{4}(p_x^2 + p_y^2) + \frac{(xp_y - yp_x)^2}{r^2}\right] + V(r, x, y), \tag{3.5}$$

where m_H represents the hydrogen mass ($m_H = 1.00794$ $a.m.u.$). The potential energy surface $V(r, x, y)$ which is calculated by Porter–Karplus [13] and the remaining expression representing the kinetic energy that is modified by Allahem [38] through Cartesian transformation to that taken from Waalkens *et al* [39].

The full system is given by

$$
\begin{aligned}
\dot{p_r} &= \frac{-\partial H}{\partial r} = \frac{1}{m_H}\left[\frac{2x}{r^3}(xp_y - yp_x)\right] - \sum_{j=1}^{3} \frac{\partial V}{\partial R_j}\frac{\partial R_j}{\partial r} \\
\dot{p_x} &= \frac{-\partial H}{\partial x} = \frac{-1}{m_H}\left[\frac{2p_y}{r^2}(xp_y - yp_x)\right] - \sum_{j=1}^{3} \frac{\partial V}{\partial R_j}\frac{\partial R_j}{\partial x} \\
\dot{p_y} &= \frac{-\partial H}{\partial y} = \frac{-1}{m_H}\left[\frac{2p_x}{r^2}(xp_y - yp_x)\right] - \sum_{j=1}^{3} \frac{\partial V}{\partial R_j}\frac{\partial R_j}{\partial y} \\
\dot{y} &= \frac{\partial H}{\partial p_y} = \frac{1}{m_H}\left[\frac{3p_y}{2} + \frac{2x}{r^2}(xp_y - yp_x)\right] \\
\dot{x} &= \frac{\partial H}{\partial p_x} = \frac{1}{m_H}\left[\frac{3p_x}{2} - \frac{2y}{r^2}(xp_y - yp_x)\right] \\
\dot{r} &= \frac{\partial H}{\partial p_r} = \frac{2p_r}{m_H}.
\end{aligned}
\tag{3.6}
$$

Because of the difficulties in visualising the geometry structure of the full system behind the reaction transition, the reaction mechanism is not clear when, for example, the entire DS is four dimensional section of the five dimensional energy surface. Due to dimensionality prospective, it is still unknown how to deal with the TS and its invariant manifolds for the system held six dimensions. The existence of reflection symmetries led to reduce the full exchange hydrogen reaction to an invariant system with four dimensions. The reflection : $x \to -x$ produces the collinear system under $y = 0$ assumption, for instance.

The reflection symmetries keep the potential energy function $V(r, x, y)$ invariant which can be seen clearly with the help of Figure 3.2. These reflection symmetries and their composition led to extend the study to phase space as their canonical transformation can be written as

$$
\begin{aligned}
P_x &: (p_r, p_x, p_y, r, x, y) \mapsto (p_r, -p_x, p_y, r, -x, y) \\
P_y &: (p_r, p_x, p_y, r, x, y) \mapsto (p_r, p_x, -p_y, r, x, -y) \\
P_x \circ P_y &: (p_r, p_x, p_y, r, x, y) \mapsto (p_r, -p_x, -p_y, r, -x, -y).
\end{aligned}
\tag{3.7}
$$

These symmetries are inherited in the Hamiltonian 3.5 that represent the collinear invariant system, where all versions of configurations to the molecule are unchanged, as a result of the hydrogen atoms were identical. This collinear system is explained in more detail below, which forms the basis of my research and a topic of huge interest.

Moreover, time-reversal invariance symmetry is also held in the Hamiltonian, that is expressed as potentials plus kinetic. This means keeping the coordinate fixed and changing the sign of momenta will drive the trajectories back in their reversed time direction. However, this kind of symmetry does not apply to any Hamiltonian. However, $+x$ and $-x$ are related by the reflection symmetry in the collinear configuration. Time reversal invariant symmetry plays a subtle role in directional flow proceeds from one side to the other. Physically speaking, forward and backward reactions are different whenever signs of the momenta are altered. This symmetry leaves the Hamiltonian invariant is clear. Time reversal invariant symmetry T can be expressed as follows:

$$T : \begin{array}{l} p_x \mapsto -p_x \\ p_r \mapsto -p_r. \end{array} \tag{3.8}$$

The reflection combined with the time-reversal symmetry leads us to address the forward and backward reactions within this thesis. This combination of symmetries can be applied to the collinear system and can be explained simply by changing the momentum sign to indicate the past of the molecule and the future evolution. This can be expressed as:

$$TP_x : (p_r, p_x, p_y, r, x, y) \mapsto (-p_r, p_x, p_y, r, x, y). \tag{3.9}$$

3.5 Hamiltonian Collinear System

In this section, the shape of the hydrogen complex will be described where the full spatial system is reduced to the invariant system, with two dof that is different in setup but is thought of its contribution to reduce the phase space. The collinear system, the key focus of this study, is explained in more detail in the next chapters 4 and 5. The hydrogen exchange reaction $H_2 + H$ is given by the Hamiltonian function (3.5). An assumption of $y = 0$ leads to the collinear case as $(y, p_y) = (0, 0)$ as a result of the following equations: Let

$$\begin{array}{l} y = 0 \to \dot{p_y} = 0 \\ p_y = 0 \to \dot{y} = 0. \end{array} \tag{3.10}$$

This means that the system is invariant collinear and can be given by

$$\begin{aligned} \dot{r} &= \frac{\partial H}{\partial p_r} = \frac{2p_r}{m_H}, \quad \dot{p_r} = \frac{-\partial H}{\partial r} = -\sum_{j=1}^{3} \frac{\partial V}{\partial R_j}\frac{\partial R_j}{\partial r} \\ \dot{x} &= \frac{\partial H}{\partial p_x} = \frac{3p_x}{2m_H}, \quad \dot{p_x} = \frac{-\partial H}{\partial x} = -\sum_{j=1}^{3} \frac{\partial V}{\partial R_j}\frac{\partial R_j}{\partial x}. \end{aligned} \tag{3.11}$$

Now, we use $x = 0$ as the dividing surface, which is the right choice. Because it implies to symmetric condition and it is transverse to the flow except at the boundary where most trajectories are laying on for all times. The dividing surface plays a subtle role in determining whether a trajectory is reactive or nonreactive.

The collinear system is a four-dimensional in phase space, and the dividing surface is then a two-dimensional sphere. The boundary of the DS (SSPO) is S^1 equator which split the PODS into two hemispheres. Thus, the disjoint union of the PODS ($S^1 equator$) and two dimensional balls (B^2) form the dividing surface [85]. The SSPO then divide the DS into two hemispheres $P_x > 0$ and $P_x < 0$. These hemispheres are similar because the Hamiltonian flow behaves similarly in each hemisphere due to the symmetry of the Hamiltonian function. As the TST determining the minimum flux through the PODS, the appearance of many PODSs indicates that the reaction rate would be overestimated [86].

Relevant periodic orbits are introduced with their properties and propagations to the collinear system carefully considered, which has the potential to aid the understanding of the appearance of nonreactive trajectories on the DS.

3.5.1 Collinear Periodic Orbits

In this section, we introduce the properties of periodic orbits and why they are important and discuss their connection to the phase space structure, in order to understand the reaction mechanism.

The collinear hydrogen reaction is characterised by the Hamiltonian equation (3.11), which admits several periodic orbits for energy just above the saddle point energy.

These periodic orbits can change the structure in phase space, such as F_1 in Figure 3.3. Combined with invariant manifolds, they can control the transport dynamics from or toward the transition state. Each periodic orbit is associated with the stable and unstable manifolds through which the flow is directed to or away from it.

However, their contributions to divide the phase space into regions can simplify the dynamical study that is already centred in configuration space. For instance, an interaction region can be determined by different manifolds emanated from different periodic orbits and cross each other, such that reactive trajectories do not enter.

In terms of the structure, the first known unstable periodic orbit (SSPO) was identified by Pechukas *et al* [31] in the hydrogen exchange system with two dof that determines the DS such that the TST rate is exact for energy up to $E \approx -4.14676$ e.V. Iñarrea *et al* [20] have calculated families of periodic orbits that exist through the energy region of interest and are emerged by a sequence of bifurcation as a result of a change in the energy parameter. He found the first bifurcation is of the saddle-node type which occurs symmetrically at both sides of the saddle point. The unstable periodic orbit F_1 and the stable periodic orbit F_2 arise by the bifurcations on both sides of the symmetric stretch periodic orbit shown in Figure 3.3.

The PODS has been studied by Allahem [41] within the centre manifold of the saddle point and described as the symmetric stretch, due to vibration mode. The Symmetric Stretch Periodic Orbit (SSPO) can divide the DS into symmetric hemispheres through which unidirectional flux pass through as a point of no return. These hemispheres can be described as forward or backward in terms of the flux reaction direction. The SSPO with its interior can be a suitable candidate to be a DS among others.

The SSPO lives in the collinear system, which undergoes a sequence of bifurcations as a result of one parameter energy change. At every fixed energy, there are a few periodic orbits of which mostly come in pairs because of the reflection symmetry inherited in the system. In contrast, the family of SSPO live on the symmetry axis and exist at each energy regime.

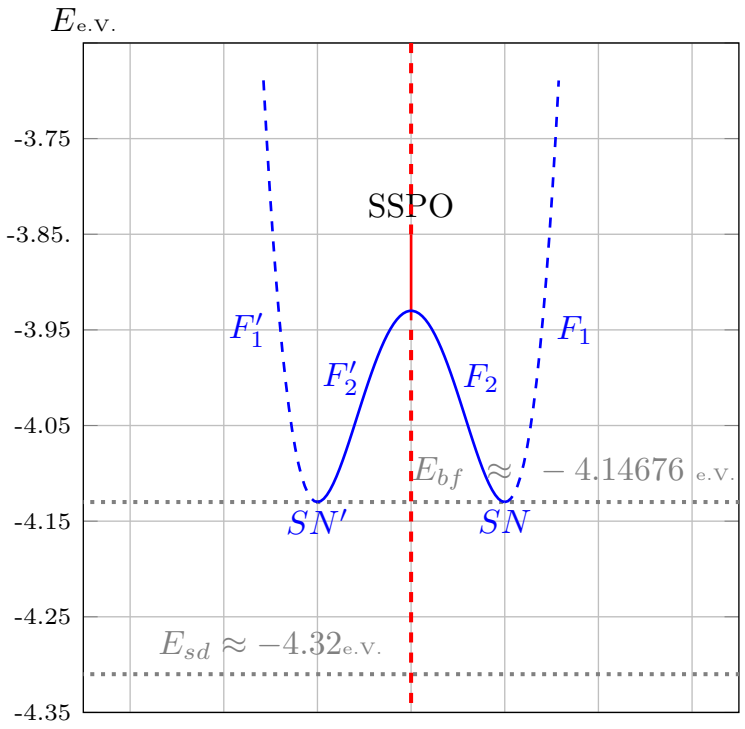

FIGURE 3.3: *Schematic the first saddle-node bifurcation diagram for the collinear system where solid and dashed lines show stable and unstable respectively. The vertical axis represents increasing energy, while the horizontal one does not refer to any quantity. E_{sd} refer to saddle point energy while E_{bf} indicates the first bifurcation energy.*

The saddle-node bifurcation creates the unstable periodic orbit F_1 on both sides far away from the SSPO and is not undergoing any further bifurcations. This is the collinear periodic orbit that is apparently connected to breaking the TST at energy interval. The saddle-node is the first bifurcation creates multiple PODSs and cause the TST to overestimate the reaction rate. This is apparently connected to our case of study and interested reader in more bifurcations referred to [20].

Most important periodic orbits created by the first bifurcation on both sides of the SSPO, which can be seen in schematic Figure 3.3. It shows that due to the system held reflection symmetry, F_1 and F_1' are unstable periodic orbits shall change the structure on the DS. The periodic orbit F_1 does not undergo further bifurcation and lives away from the symmetric reflection axis where the SSPO undergoes several bifurcations as a result of energy parameters change.

Other orbits, like the family F_2, generated by the first bifurcation, undergo a period-doubling bifurcation at $E \approx -4.146$ e.V, resulting in a change to their stability. These orbits are involved in between the first unstable periodic orbits (family F_1) that are of the most interest to transportation.

3.6 Motivation and Known Results

In 1979, it was well known that the TST rate is highly accurate related to lab calculation in quantum chemistry for the collinear hydrogen reaction such that single periodic orbit existed and bound the transition state. The recognition of this is attributed to Pechukas and Pollak [87] for an energy interval above the saddle energy value. The authors claim that a lower bound can be achieved under certain assumptions but depends on whether those trajectories are reactive. Most recently, Krajnák *et al* [88] managed to decrease reaction rate based on the Davis' proposal and using the famous Monte Carlo method. The lower bound for the hydrogen exchange reaction can be traced in [87] where the authors used a stable periodic orbit to construct a DS through which reactive trajectories cross all TSs once.

In 1987, the collinear hydrogen exchange reaction was studied in phase space by Davis [34]. The transition structure is considered under the role of invariant manifolds. Investigation for understanding the structure over three energy regions was based on the TST being exact, as a result of a single periodic orbit representing unique TS, while several periodic orbits represent multiple TSs at higher energy. Like Pechukas and Pollak, he elucidated the structure, that is invariant and relatively simple by means of invariant manifolds techniques. There are four invariant manifolds which drive the system forward and backwards to the symmetric stretch periodic orbit. These manifolds Davis calls separatrices and terms adapted to stable and unstable manifolds.

When more periodic orbits occur at a range of higher energies, the structure becomes complicated rather quickly and would not help in understanding the transport mechanism. As mentioned by Davis, there are five periodic orbits in the collinear hydrogen reaction. The symmetric stretch and (collinear) outermost periodic orbits (family F_1)

represent a TS each until the former one turns to be stable at high energy. There are also secondary periodic orbits shown in Figure 3.3 at both sides of the symmetric stretch, in between the two TSs. The symmetric stretch bounds the DS in our study, which lost its normal hyperbolic before being restored to imply the TST structure in phase space.

Davis' resolution is based on that an interaction region is bounded by stable and unstable manifolds of different periodic orbits, which distinguish between reactive and nonreactive trajectories for a range of energies interval. However, there is a particular energy value of $E = -4.141$ e.V., where the interaction region can be constructed above the first bifurcation energy, which is the point of interest. The symmetric stretch separatrix is invariant since no other separatrix branches cross them. This means the flow volume is separable by the separatrix, and no heteroclinic point is found. Davis' hints of that there exist many invariant curves between the two PODS which led us to find one of them and explain its influence on transport in the collinear hydrogen system, as well as its effect on the DS reactive islands. Most recently, Krajnák provides more details about the interaction of invariant manifolds and their crucial role in understanding heteroclinic existence. These heteroclinic tangles are known to be created between two different periodic orbits, as a result of their manifolds intersect each other on a heteroclinic point at a specific energy value. These tangles were studied by Davis, who found that their size grew as a result of an increased energy value given to a portion of trajectories that do not react. However, Allahem [41] found that the collinear periodic orbit (F_1) causes the TST failure but not in a precise manner. We explain this in more detail employing the linear approximation techniques and reactive islands.

Recently, Allahem[41] hypothesised that nonreactive trajectories are separated from reactive trajectories by invariant manifolds associated with a collinear (unstable) periodic orbit (F_1). Motivated mostly by a recent study launched by Allahem [41] leads us to describe a phase space object thought of its relation to the breakdown of the TST. In particular, collinear periodic orbit $F1$ is unstable over a particular energy region where multiple PODSs violate the concept of TST in the collinear Hamiltonian dynamical reaction system. Our main aim is to describe its relation to the phase space structure qualitatively via the invariant manifolds theory as well as the transport reaction

mechanism via reactive islands.

Reactive islands can be defined as a projection into two-dimensional space to the central sphere using Poincaré surface of sections. The central sphere is the symmetric stretch (unstable) periodic orbit that vibrates between the equipotentials and that bounds the bottleneck through which the system must pass during a reaction. The reaction can be identified as forward or backwards based on the sign of momenta that is conjugated to the reaction path. These identifications produce either forward or backward DS (the central sphere). As the DS is filled with reactive and nonreactive initial conditions, the reactive islands consist of layers that can be reactive or nonreactive, respectively.

Most recently, Allahem [41] studied these islands and found the boundary of the main nonreactive islands by means of linearization to the stable manifold of the collinear (unstable) periodic orbit, denoted as F_1, at prescribed energy value $E = -4.141$ e.V. He found those trajectories launched nearby the F_1 cross the DS and lying on the boundary of the nonreactive islands which is called by the stable intersection. The stable intersection curve bounds the main nonreactive layer of the reactive islands on the forward DS, as presented in Figure 4.6. The recognition of this work is attributed to Allahem [41], who used Mathematica, which is confirmed by Matlab simulations in the next chapter 4.

Beyond Allahem's achievement, our contribution gives more detail and new results about the boundary of different nonreactive layers. Not only it confirms his result but also drive our attention to find the mirror image of the nonreactive islands in the backward DS where the unstable intersection is explained later. This gives new techniques to find the symmetric stable intersection.

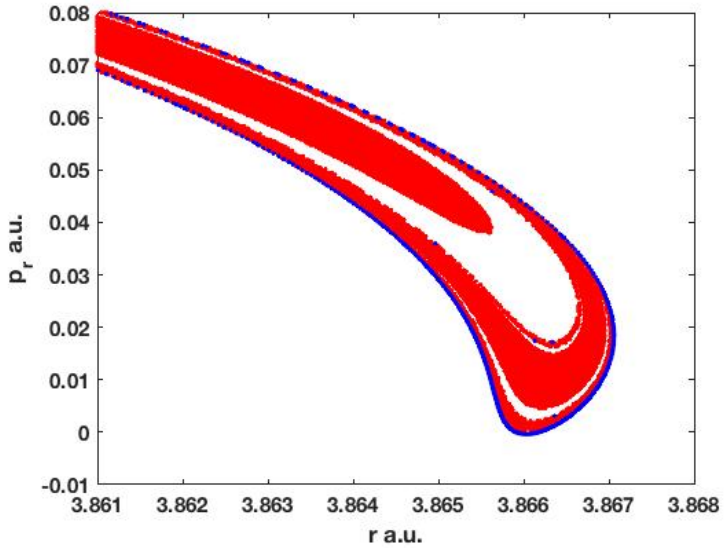

FIGURE 3.4: *Points (blue) on the stable intersection lies on the boundary of the main nonreactive islands (red) at* $E = -4.141$ *e.V.*

Chapter 4

The boundary of Reactive Islands

4.1 Introduction

A reactive island plot gives a simple projected picture to represent reactive and nonreactive initial conditions (IC's) in the DS for the collinear hydrogen reaction. De Leon and Marston [89, 90] were firstly studied their geometrical shapes for the isomerisation reaction model. In the collinear hydrogen exchange reaction, Pollak and Child described the shapes which are called "droplets" by Davis [37]. Recently, Allahem [41] studied the collinear hydrogen reaction using reactive islands plots and demonstrated the emergence of nonreactive droplets in the DS because the collinear periodic orbit F_1 interfered with the role of the symmetric stretch periodic orbit explained in this thesis. We aim to explain how such shapes appear in the DS located between reactants and products, identifying them and their structure which is affected by the collinear periodic orbit F_1 that is located off the saddle barrier site in the reactants side.

Molecular dynamics simulation has been employed for studying the collinear exchange hydrogen system. In the collinear Hamiltonian, the potential energy is restricted to be smaller than the total energy. In other words, if the potential energy was higher than the total energy, the system will be complicated. Evaluation of how reliable a

numerical solver is investigated based on the performance of a computer with finite-precision routine and a topological dynamical property will be studied in section 4.2.

The purpose of this chapter is to study the boundary of reactive islands on the DS. This study will be for the collinear system case. This would be useful when we establish the invariant manifolds mediating the reaction dynamics in Chapter 5. Our main goal is to find a boundary for each nonreactive droplet. This type of study has been carried out further, as explained below.

In what follows, Matlab numerical solvers will be assessed, and the reactive islands plots at different energy values have been demonstrated. We observe whether there are any qualitative changes in the structure of the reactive islands and compare these to the first bifurcation of the periodic orbits in the barrier region, as studied by Iñarrea and Salas [20]. The stability analysis of F_1 allows us to use the linear approximation, in order to find the stable manifold of F_1 described in section 4.4. The slightest small deviation is used in propagating trajectories on the linear approximation of the stable manifold in the back-time direction. The surface of section is located at the DS to find where the un/stable manifolds are crossing the DS. This study is also essential to investigate the dynamics in the vicinity of F_1 explained in Chapter 5. After that, we will demonstrate the intersection of the unstable manifold of F_1' to the DS, relate it to the stable manifold of F_1 intersection studied by Allahem [41].

At this point, we can determine a phase space region that is related to this study, regarding finding the boundary to several nonreactive layers in the DS.

4.1.1 Interaction Region

In this section, we determine a phase space region in phase space related mostly to the bottleneck where the hydrogen atoms collide and perhaps exchange configuration. In configuration space, this region contains the saddle point where the potential energy barrier is located. Reactants and product asymptotes can be determined on both sides of the region as far as one hydrogen goes to infinity and does not react. To dive into the transition structure, we shall call the region in phase space which contains the SSPO

and F_1 periodic orbit as an interaction region. It is apparent that the collinear periodic orbits F_1 and its image F_1' destroy the symmetric configuration of the natural transition state at the saddle point. Due to its existence at the furthest side of the SSPO, the interaction region is defined to be between the SSPO and F_1, unless otherwise stated. Advantages of this interaction region are immediate:

It includes all other periodic orbits such as F_2 at higher energy values than the bifurcation energy and is the most appropriate choice for our numerical evaluation, based on Allahem's claim [41].

This region is also defined on the product side of the configuration space that is symmetric to its respective reactant side. These sides are carefully equivalent and have similar dynamics in the collinear hydrogen reaction. When we compare between these regions in order to determine the invariant manifolds, which substantially influence the appearance of the nonreactive islands on the DS, as well as cause TST failure, it is reason enough to choose the interaction region between SSPO and F_1.

There are four manifolds branches emanated from different PODSs launched in the interaction region, and there must be among those branches which shall cause the nonreactive islands to appear in the DS. Those are either the stable or the unstable manifolds of the collinear unstable periodic orbits (family F_1) since the SSPO and their separatrix branches are invariant in the sense that no flux across them. Thus, we are looking for invariant curves lying between and not across the SSPO's separatrix branches, as stated by Davis [34] at energy value equivalent to ours at -4.141 e.V.

Computer ode solvers will now be tested in order to establish which of these ode solvers will be used in this thesis.

4.2 Evaluation of ODE solvers

Numerical computations play key roles in studying the Hamiltonian collinear system by solving the equations of motion across several simulations. In this section, we will test Matlab solvers based on the previous finding of the stable intersection against invariant

property inherited in any trajectories. If we restrict a trajectory to be propagated in the interaction region forward and backward evolution. For that, we need to define the surface of section on the boundary of the interaction region. Before that, we will give some useful information regarding our argument.

In particular, we will identify a numerical solver in Matlab for use throughout this research. The evaluation is based on computer performance, to obey the invariance condition that every trajectory starts within manifold will stay on that manifold for the future as well as the past evolution. This invariant property facilitates our assessment and understanding of the complicated behaviour of the trajectories that will be started nearby the F_1 and then propagated back to across the DS. Because of the stable intersection bounds the main nonreactive layer of the $E = -4.141$ e.V. reactive island on the DS which is confirmed and agrees with previous studies [41]. Our approach is based on the invariant property that every trajectory on the stable intersection is expected to return back to the F_1 when the time span is reversed.

In this section, we will test ordinary differential equation (ode) solvers that are provided by Matlab such as $ode23, ode45$ and $ode113$. We will choose an appropriate solver to use throughout this research. Our test is based on that all trajectories on the stable intersection are expected to return back to their destinations in reverse direction. Every trajectory is an invariant set that starts and remains within the set for future and past evolution. First, we start at the stable intersection curve and propagate the involved trajectories in forward time toward F_1 direction. We expect all trajectories in this set to return back to F_1 side.

Therefore, the region of interest is located between the SSPO and the periodic orbit F_1, which contains all other periodic orbits of the collinear hydrogen system restricted to one side of the symmetry axis. This is an excellent choice to delimit the symmetric “effect ”that may violate the test. As the stable intersection has been found by propagating trajectories nearby F_1 backwards, one may reverse the simulation forwards and observe that all trajectories return back to their initial values is a proper challenge. This can be seen by locating a suitable Poincaré Surface of Section (PSS) as close as enough to the F_1 location such that a suitable tolerance is used.

This situation shows that not all trajectories on the set return back to their destinations when the surface of section located at $x_* \in F_1$ for $ode45$ simulation. Therefore, the correctness of the simulation is carried out by choosing a Matlab solver, such as $ode23$, for crude tolerances, or modifying the tolerance over such solver. Matlab has underlying solvers that compute numerical solutions for several types of dynamical systems. These algorithms are stored as functions to determine the solution at a prescribed accuracy. For example, $ode23$ estimates the step size required by comparing the second order with third-order methods in order to obtain a prescribed accuracy. The numerical simulation shows that not all trajectories on the stable intersection return back to their starting points as the time direction is reversed.

One can use this technique in order to increase accuracy among simulation. Correctness among such numerical relative errors control a computed answer with the correct number of digits ($RelTol$). However, our goal is not to compute an approximated solution that agrees with the desired accuracy but to obtain crossing points within a specified tolerance. In order to detect such an intersection point, the tolerance has to be higher than the solution component, and so generally the solver controls an approximated solution automatically. For example, if the tolerances are increased, the accuracy of the solution and the runtime are increased, and vice versa.

The numerical methods implemented in Matlab estimate the absolute error between the approximation solution x_0 and the exact solution x in general. However, when the approximated solution is near to zero, the relative error will be undefined, and the solution has no correct significant digits. In this case, tolerance grows to infinity, and absolute tolerance is used. This kind of limitation implies that the error at each step of the solution component is growing. Observation shows that absolute error tolerance controls the approximation solution when the surface of a section at $x_* \in F_1$ is detected as follows.

The absolute error is written as

$$err_{abs} = |x_0(j) - x_*|.$$

To improve accuracy, either relative tolerance or absolute tolerance is chosen, according to which one is governing the integrator. Firstly, the code is executed within the default relative tolerance and then checked:

if $x_0 > AbsTol \mapsto$ relative tolerance is used,

or

if $x_0 \leq AbsTol \mapsto$ absolute tolerance is used.

In general, ode solvers use different methods for computing each component of the solution when the local error inside the integrator is controlled. For those particularly interested in this matter, refer to Matlab documentation and [91] from where most of the above information about tolerance has been taken.

Now, the reliable ode solver will be identified, based on the performance of numerical computations that feed into the topics of this thesis. We shall start by three types of ode solvers such as *ode*113 , *ode*45 and *ode*23. The *ode*45 and *ode*23 are similar methods, based on the different orders of the Runge-Kutta formula, compared with *ode*113. The *ode*113 method evaluated the solution at variable orders of accuracy. This is known as an efficient method when the computation is expensive. While the other methods are considered as the higher orders, which takes larger time steps for each workload, we applied these methods to the stable intersection sample and propagated their ensemble of trajectories in forward time direction towards $x_* \in F_1$, where the initial points generated for the stable intersection calculated by Matlab.

The expectation was for all trajectories to return back to their original initial points by at least σ_s digit numbers tolerance. However, this is not always the case because propagating trajectories toward unstable periodic orbit leads to complicated behaviour. An *ode*23 requires longer running time than *ode*45 and *ode*113 but has given a solution as accurate as *ode*45 which is shown in Figure 4.1. Also, if the tolerance is increased, *ode*23 will take a long time to give an answer, in comparison with the other ode solvers. Note that, the default setting for all solvers is 10^{-3} for relative tolerance and 10^{-6} for absolute tolerance. Accordingly, *ode*113 return 95% trajectories while approximately a third quarter of trajectories are preserved under the ode45 simulation. For achieving the desired solution, these percentage will decrease, unless the tolerance is met.

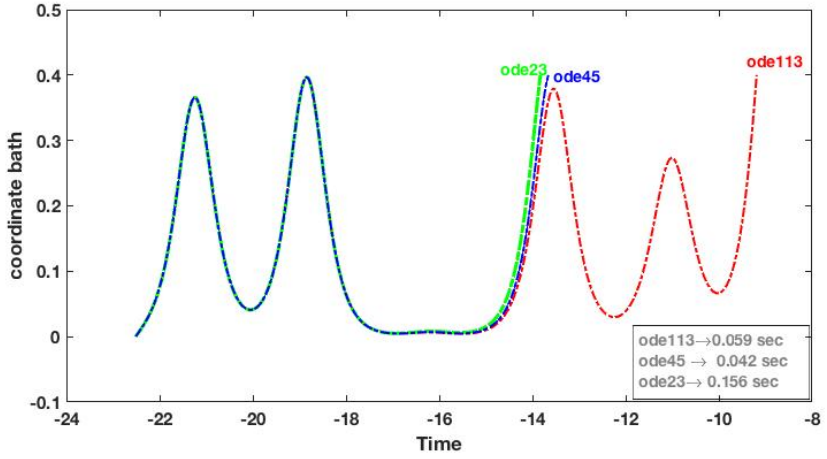

FIGURE 4.1: A trajectory propagated forward by *ode*45, *ode*23 and *ode*113 with the same tolerance as the one used to propagate them in backward time toward the DS.

Figure 4.2 shows a linearised trajectory propagated back and forward in time toward F_1 and the DS respectively, by *ode*113 and *ode*45 for comparison. The *ode*45 has the same setting as the *ode*113. Our evaluation is based on several steps: firstly, we start with zero-crossing and default relative tolerance in both directions until the trajectory preserved. Then, we propagate the linearised trajectory backwards and forward in order to cross the surface of the section, as shown in Figure 4.2. The *ode*113 trajectory go forth and back with a relatively smaller error that is shown in the top panel related to *ode*45 shown in the bottom panel of Figure 4.2.

Then, we changed the relative tolerance on both simulations and found that *ode*45 trajectory diverges from that in the middle on one side while the *ode*113 results diverge in a different direction as shown in Figure 4.3. However, the *ode*45 was unable to meet integration tolerance at $10^{-}9$ relative tolerance. However, in any simulation, the time step size and tolerance can show if the simulation is stable. For example, if one changes from relative tolerance 10^{-6} to 10^{-9} and quickly find that the two results are pretty close as it can be seen on the first panel for *ode*113 in Figure 4.2. Also, as we increase the number of time steps in the direction of one variable, the approximated solution converges to the surface of the section. Although *ode*45 should be the first one to try in

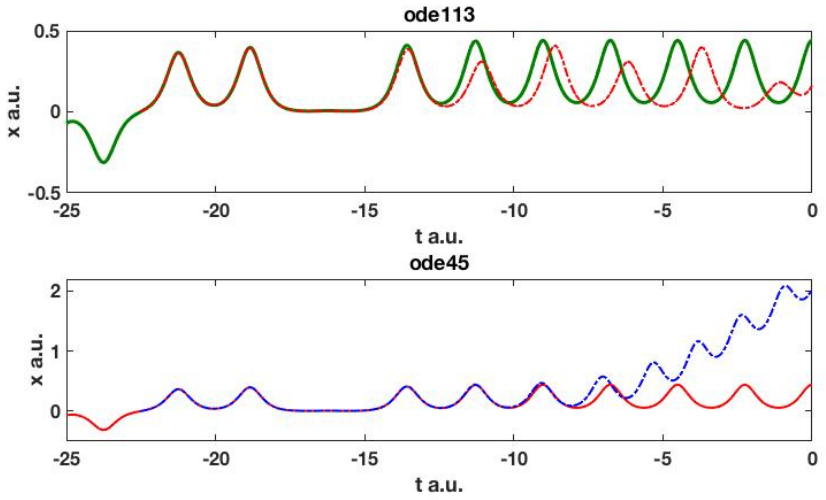

FIGURE 4.2: The trajectory propagated by *ode*113 on the top panel and *ode*45 below with the same tolerance for both simulations in the backwards and differ in the forward as explained in text.

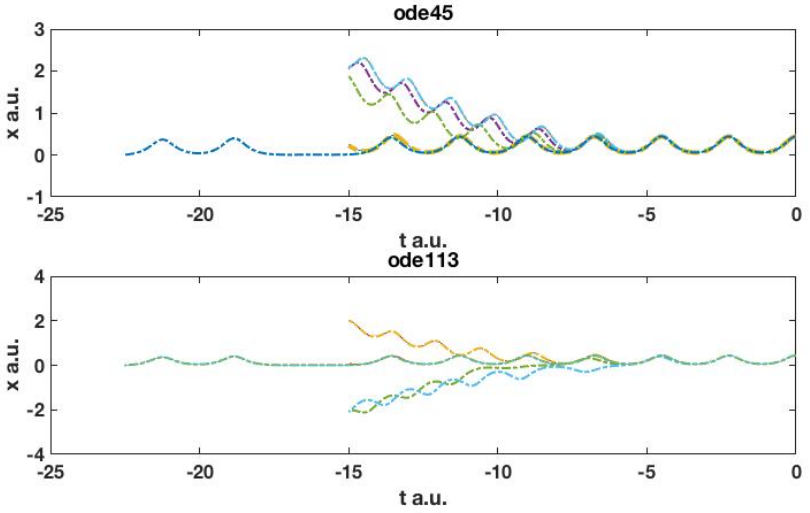

FIGURE 4.3: The trajectory propagated by *ode*113 on the top panel and *ode*45 below with various relative tolerance on both simulations. Note that the middle trajectory is the same as the one presented on Figure 4.2.

any numerical simulation, *ode*113 can be the most efficient solver when accuracy differs. As a result, *ode*113 is the reasonable choice to be used in this research.

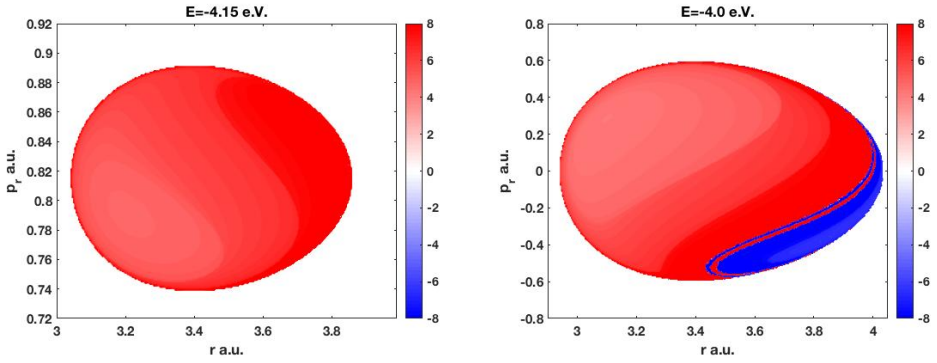

FIGURE 4.4: *The reactive (red) and nonreactive(blue) islands on the dividing surface for different energy values. Initial values have been chosen for energies* -4.15 *e.V. (before the first saddle node bifurcation of PODS), and* -4.0 *e.V. respectively.*

4.3 Bifurcation Effect on Reactive Islands

In this section, we demonstrate reactive islands of the DS at different energy values before and after the first bifurcation. We will explain how the structure is differed and caused the nonreactive island to increase in size as energy value increases. How these droplets appeared in the DS at a particular energy value will be the core of this research.

A numerical simulation has shown that all regions of the DS are covered by the only reactive island and no appearance of nonreactive islands at energy value of $E \approx -4.15$ e.V., which is less than the first bifurcation energy occurred at $E \approx -4.14676$ e.V. Above the threshold, nonreactive islands start to appear in the DS. These results are illustrated in Figure 4.4.

These results are shown in Figure 4.4 where only single PODS governs the system at energy value $E = -4.15$ e.V. However, several PODSs exist at energy $E = -4.0$ e.V., which is above the first bifurcation. In order to show how the nonreactive droplets increased in size, we pick an energy value at $E = -4.1$ e.V. in between the previously selected energy values. The size can be seen in Figure 4.5 where there are fewer nonreactive trajectories than those observed at $E = -4.0$ e.V.

Having said that as energy increased, more trajectories can pass through F_1 into a complicated region where the stable manifold of F_1 separates reactive trajectories from those

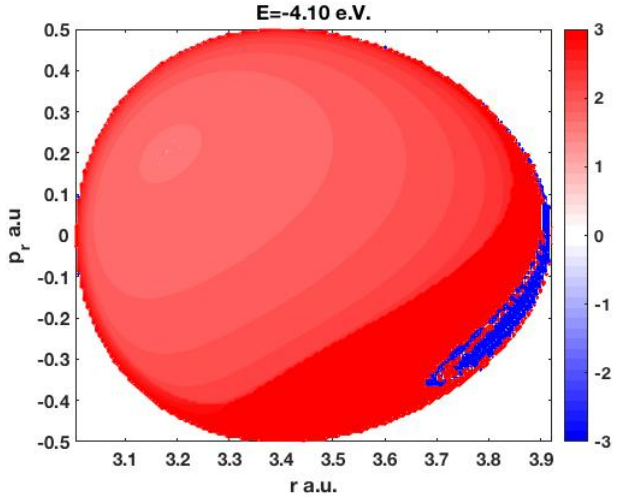

FIGURE 4.5: The Reactive islands at E≈ −4.10 eV.

re-crossing the SSPO or even nonreactive ones. Thus, the new (collinear) PODSs govern the system passing through to the SSPO. Davis [34] observed that those trajectories enter the homoclinic region and eventually re-cross the barrier while reactive ones miss that region and cross the barrier only once. Therefore, widening the gate will lead to more nonreactive trajectories projected on the DS. It is also important to note that the outer PODSs are the outer doors for the SSPO. Locating surfaces of section far away from the outer periodic orbit F_1 would be reasonable but will not always be useful, as each periodic orbit represents a TS itself.

However, when the outer periodic orbits come close to the symmetric stretch, the latter lost its normal hyperbolicity before regaining it again as the former periodic orbits stay away apart. At energy where the SSPO undergoes bifurcation, the reason explaining how nonreactive islands appeared on the DS, is still unexplained very well. These islands enclose nonreactive trajectories that are reflected back by F_1 and F_1' with equal translational energy.

These periodic orbits can be seen as opposite wheels driving the system back and forth towards the SSPO through their separatrix branches. Their connections to bound nonreactive layers in the DS are explained below in more detail.

The flux volume can be determined through the F_1 and F_1' along to the SSPO. These periodic orbits can reduce the volume through to a minimum or maximise the flux leading to the SSPO. For instance, the PODS still holds the leading role to determine the flux volume direction through the F_1. This is reasonable enough to persuade us to consider the stable manifold of F_1 in order to produce the stable intersection and similarly for the unstable intersection that is approximated linearly from the unstable manifold of F_1' described below.

Now, we shall start by introducing the linear approximation for $E = -4.141$ e.V. by means of the monodromy matrix's eigenvalues corresponding to their prospective stable and unstable eigenvectors used to find the stable and unstable intersections.

4.4 Stability Analysis of the Collinear Periodic Orbits

The appearance of the collinear periodic orbit F_1 leads us to see if it is stable or unstable, the monodromy matrix $M(t)$ can measure its stability type with least period T. This is in addition to checking whether a change in the initial condition leads to a change in the solution.

Consider a periodic orbit Γ with $\gamma(t)$ which is the parameterisation with period T, $M(t)$ is the monodromy matrix satisfying the variational equation.

$$\dot{M}(t) = JD^2H,$$

where J is the Poisson matrix, with the initial condition

$$M(0) = I.$$

The monodromy matrix can be defined as $M = M(T)$. It measure how an initial deviation ξ from $\gamma(0)$ change after a period T. If ξ is infinitesimally small along the periodic orbit Γ, then after a full period $M\xi = \xi$ and hence ξ is preserved.

A study concerns the stability of the Hamiltonian system suggests that there are six eigenvalues with non zero real part around the periodic orbit F_1.

Those eigenvalues found by means of the monodromy matrix at the point $x_* \in F_1$.

Since two multipliers are always equal to one, because of their corresponding Floquet exponents that are equal to zero, therefore, by deleting their columns and rows in the monodromy matrix, we can determine which invariant manifolds associated to each multiplier as follows :

If the multipliers λ such that

- $|\lambda| < 1$ corresponds to the stable manifold.
- $|\lambda| > 1$ corresponds to the unstable manifold.
- $|\lambda| = 1$ will corresponds to the centre manifold.

In terms of dimensionality, the full system is six dimensions which can be reduced to a four-dimensional collinear system. According to the multipliers, there is a stable manifold, unstable manifold and centre manifold. Since the remaining multipliers belong to the derivative of the Poincaré map, then the system will be off one dimension. Thus, the stable manifold of F_1 is one dimension as the same as the unstable manifold while the centre manifold is a plane ($2D$ surface). These manifold are tangential to the linear subspaces according to their multipliers.

The multipliers suggest that the stable manifold is spanned by the eigenvectors associated with modulus multiplier less than one, while the eigenvectors with modulus multiplier more than one span the unstable manifold. These definitions can be extended to the Hamiltonian system based on that used for the linear approximation.

4.5 Stable Intersection

The stable intersection is the intersection of the stable manifold of the collinear periodic orbit F_1 with the DS. This notion is used by Allahem [41] who found that a set of trajectories are crossing a PSS at the boundary of the main nonreactive islands. Building on his finding, we confirm that, but in more detail, and extend the study in order to fully understanding the creation of other nonreactive layers on the complicated phase space region. We shall begin by introducing the stable manifold of F_1 to the collinear Hamiltonian system.

This is basically for sufficiently small enough variation $\sigma_s \in \mathbb{R}$ in the linear approximation given by:

$$S_m = x_* + \sigma_s \, v_s \,, \tag{4.1}$$

where S_m represents all initial conditions that create the stable manifold of F_1 in forward time direction. Let x_* be a point belonging to the F_1, which is located on the interaction region. Therefore, any trajectory near the stable manifolds will move in forward time toward x_*.

Note that, in a particular direction of time, only one manifold can be computed. In other words, if we start a trajectory near some unstable periodic orbits and propagate it forward for a long time, we are going to see the unstable manifolds because the stable manifold will shrink toward the F_1 before damping away. To create a stable manifold of F_1 that crosses the dividing surface at $x = 0$, we need to propagate trajectories of (4.1) backwards in time. Varying σ_s has an essential impact in creating the stable manifold. If the σ_s values are too small, this will lead to numerical errors increasing as the computation takes long times (because the periodic orbit is unstable).

The stable manifold of F_1 will eventually intersect the DS at the boundary of the various reactive islands. The intersection points will be called a stable intersection. The stable intersection is the boundary of the nonreactive main layer of the reactive islands, as shown in Figure 4.6. However, some trajectories on the stable manifold of F_1 would not cross the DS while others could cross it as they are propagated backwards in time toward the DS. Figure 4.6 shows points on the boundary of the nonreactive main island.

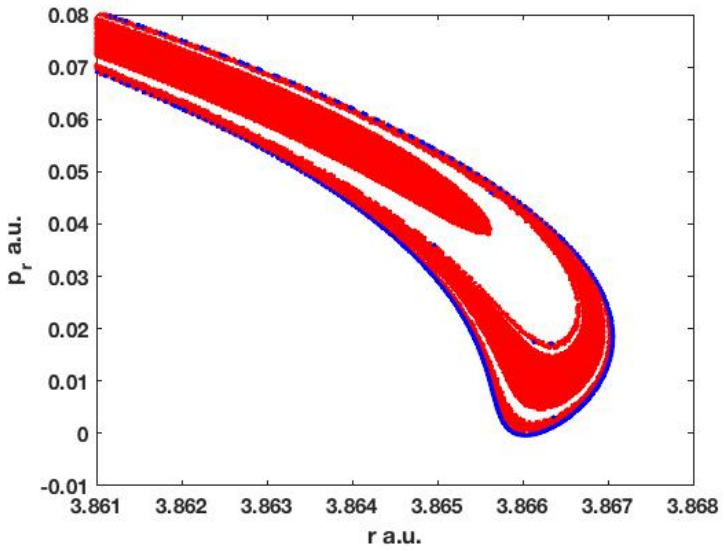

FIGURE 4.6: *Points (blue) on the stable intersection lies on the boundary of the main nonreactive islands (red).*

In fact, the simulation shows these trajectories generated by σ_s varies on the interval $(9 \times 10^{-6}, 10 \times 10^{-6})$. New ideas and questions are raised in order to confirm Allahem's [41] finding in the reflection region. Does the stable intersection bound nonreactive islands in the counterpart hemisphere or the unstable manifold of F_1' does so? This leads us to find the unstable intersection that is expected to cross the DS on the boundary of the main nonreactive layers. The linearised trajectories propagated near F_1' in forward time direction shows that the backward time direction used for the stable intersection is valid. The new finding has introduced a new technique in order to find a stable intersection, by means of the unstable intersection. The whole picture must be seen in order to understand the dynamical impacts of both collinear periodic orbits in directing the flux to and away from the DS.

4.6 Unstable Intersection

Similarly to the stable intersection, it is easy to find the unstable intersection. We pick initial values near the unstable manifold of the mirror image of the unstable collinear

periodic orbit F_1' and propagate them forward in time toward the dividing surface (DS). Then, we look for the linearised trajectories that cross the DS at the boundary of different nonreactive islands in the forward hemisphere.

In contrast to the stable manifold, all sets of trajectories moving forward in time are directed toward the SSPO and represent the unstable manifold of F_1' that can be created by:

$$U_m = x_* + \sigma_u \, v_u \,, \tag{4.2}$$

where v_u is the unstable eigenvector and the small variation $\sigma_u \in \mathbb{R}$, along the unstable manifold.

Moreover, time-reversal symmetry also holds in the collinear configuration. This means that if we keep the coordinate fixed and change the sign of momenta, the trajectory will be driven back in its reversed direction. This kind of symmetry can explain how the unstable manifold of F_1' bound the nonreactive droplets on the forward hemisphere.

Taking advantage of the combination of reflection and time-reversal symmetries, Figure 4.7 shows the unstable intersection points lying on the boundary of the nonreactive island of the forward DS as expected.

The process shows how reactive trajectories evolve in time as these families of periodic orbits approached. It turns out that some trajectories go around the F_1' many times before going back to their prospective reactant side while others cross the DS and have another trip around the F_1 before going either to the product side or returning back to cross the DS again in their journey back to the reactant side. Therefore, not only the unstable F_1 but also its image F_1' control the dynamics and are recognised to be the reason for the TST failure.

Figure 4.8 shows reactive and nonreactive trajectories in their future and past evolutions. Initial values have been chosen on the DS ($x = 0$) and their trajectories are propagated forward and backwards in time in order to cross a surface of section $\pm x \neq 0$. If a trajectory crosses $+x$, then it is reactive. If not, it is nonreactive. Backward time direction

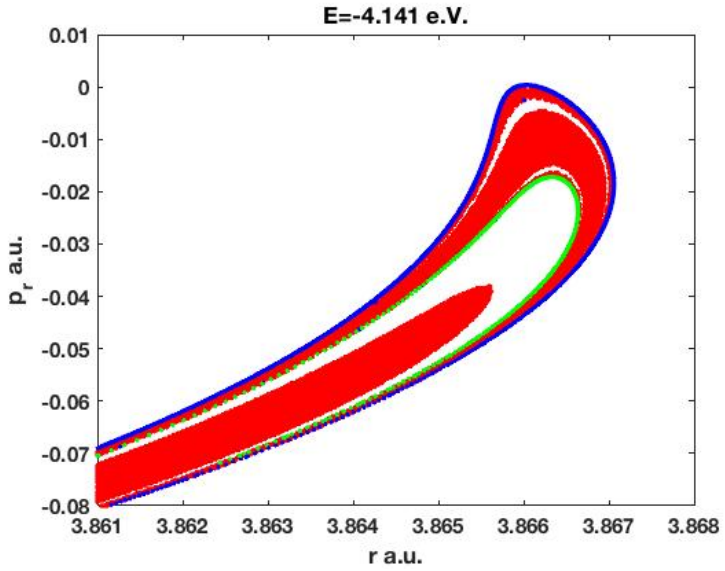

FIGURE 4.7: *Points (blue) on the unstable intersection lies on the boundary of the mirror image of the main nonreactive islands (red). Green points refer to the boundary of another layer.*

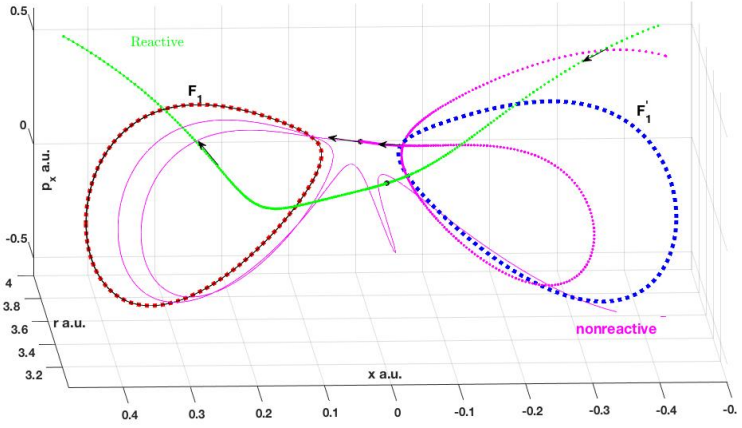

FIGURE 4.8: *Reactive and nonreactive trajectories under the dynamic controlled by F_1 and F_1'. Arrows indicate time direction, and the black dot refers to the starting point. (Details in the text).*

is used to explore which side the trajectory departure. Notice that the nonreactive trajectory has proper motion in the forward time direction, such as a cusp probably, and changes its rotation direction as it flows close enough to F_1'.

The stable and unstable intersections represented in Figure 4.9 in order to show their

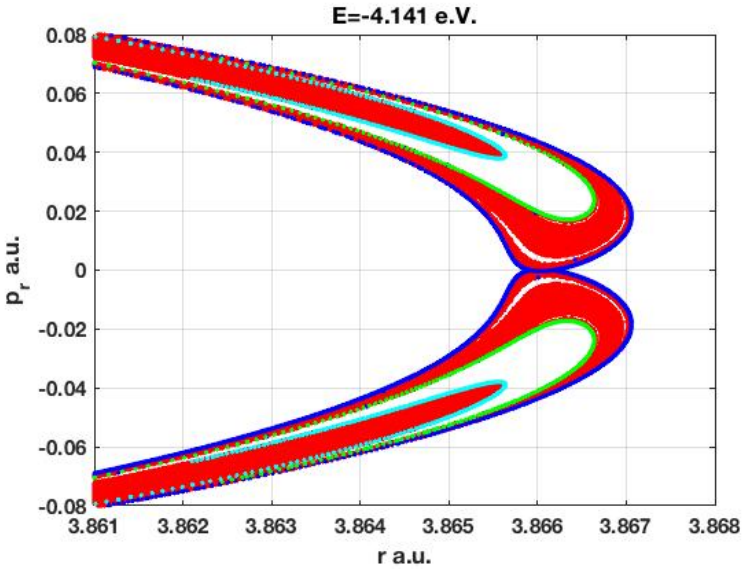

FIGURE 4.9: *The relationship of symmetry between the stable intersection (above) and unstable intersections (down). Note that both of intersections lie on the forward hemispheres.*

connection. These intersections are connected by time-reversal invariant and reflection symmetries. The inner boundaries can be generated using these symmetric properties such as σ_s for the stable and σ_u for the unstable manifolds. This new technique helps us to find the stable intersection by means of the unstable intersection and aid the study of the transport mechanism to and away from the SSPO.

It is worthy to note that these nonreactive droplets are projected on the forward hemisphere of the DS where they are expected to overlap each other in a region close to the vicinity of $p_r = 0$ as shown in Figure 4.9. These trajectories belong to that overlap region are expected to obey the TST such that they start on the reactant side and propagate toward the DS in order to reach the product region. Also, if one follows the ensemble of trajectories creating the upper nonreactive droplets, these trajectories are corresponding to the reactant region in their past evolution and return back to the reactant area as they are propagated in a forward time direction. In contrast to those trajectories contained on the lower nonreactive droplets, if one follows these nonreactive trajectories in their backward time direction, they are corresponding to the product side on their past and future evolutions. By symmetry, the mirror image of the stable intersection will bound nonreactive droplets in the backward hemisphere on the DS while the

symmetric unstable intersection will lie on the boundary of nonreactive droplets existed on the backward hemisphere symmetric to that presented in the forward hemisphere. These droplets cannot be shown on one figure due to the convention made on one side of the symmetry axis.

Chapter 5

Chaotic Dynamics in the Collinear System

5.1 Introduction

As addressed in the previous chapter 4, nonreactive droplets may open up in the DS of the collinear Hamiltonian system. The emergence of these droplets is connected to the stable or unstable manifold of the collinear periodic orbits launched from the product or reactant side to across the barrier centred in the configuration space. Therefore, the stable intersection bounds the various nonreactive layers on the forward DS while the unstable intersections bound those layers projected on the DS on the backward time direction.

In classical dynamics, chaotic scattering plays essential roles in numerous applications in nonlinear physics which have been checked in many fields such as atomic and nuclear physics, fluid and celestial mechanics and others [92]-[93]. The work provides an account of the physical phenomenon of chaotic dynamics where our attention has been focused on the most contribution related to the boundary of nonreactive islands. One of the complicated examples is those nonreactive trajectories recross the DS and return to their origin. Such motion is unpredictable in a periodic Hamiltonian system. These

trajectories represent the particles' path where the incident particles move on straight line far enough from the outside of the scattering region and interact with the scatterer (potential) [94] before leaving to either reactant or product regions.

Miller and Rankin [95] found that small changes in the initial conditions lead to different evolutions result in different final states. So that, nonreactive trajectories may land in the vicinity of reactive islands or vice versa. However, the unstable periodic orbit has been emphasised in [31] resolves that for a certain amount of energy before collapsing to do so at higher energy values. Later work [96] showed that there exist an infinity periodic orbits bounding a nonattractive chaotic set. An interesting development regarding the control of chaos using the unstable periodic orbit can be traced in the work of Ott, Grebogi and Yorke [97, 98] and [99],[100]. Here, the motion is not chaotic and can be stabilised by a sufficiently small deviation.

In our case of study, the scattering is nonchaotic because the total energy E is larger than the potential energy of the particle at the peaks. However, the chaotic saddle contains unstable periodic orbit which never leaves the scattering region. On the other hands, the potential surface contains lots of unstable periodic orbits such as the collinear unstable periodic orbits emerged by the first bifurcation. These periodic orbits constitute the chaotic set formed by the intersection of their stable and unstable manifolds. These manifolds are invariant set, and so their intersection is invariant, every orbit starting in the chaotic set, never leaves the set.

In this chapter, we are going to study the difference between trajectories on the stable manifold that cross the dividing surface and those that do not. We will obtain trajectories as close as possible to the boundary between crossing and non-crossing trajectories and show their behaviour. We will document that inner layers of the nonreactive islands are not produced by trajectories crossing the dividing surface repeatedly. After that, we will display the number of intersection points for various trajectories on the dividing surface and elucidate the relationship with the reactive island's structure. Finally, we will study the invariant manifolds of the collinear model utilizing a Poincaré surface of section transverse to the collinear periodic orbits and show their heteroclinic intersection.

5.2 Transport Dynamics

Transport dynamics enhance authors to find whether the optimal PODS (2 dof) exist or not. The geometrical structure in phase space is also well understood at low energy values. However, the trajectories' motion is affected by many invariant manifolds in order to influence transport phenomena in nature. These invariant manifolds are the three unstable periodic orbits in phase space at $E = -4.141$ e.V. Each periodic orbit can be elected as a PODS through which the flux evolve in and out along or nearby their respective stable and unstable branches. We shall call these branches as inner or outer in respect to their expected evaluation toward the SSPO or away from F_1 and F_1'. Note that the outer branches are in the products or reactants asymptotes.

Davis *et al* [34], however, stated that the SSPO's separatrix branches are invariant in a sense no flux across them. Even though, they mentioned that there is at least four flux in and similar flux out evolved from those four branches belonging to the SSPO, inner branches emanate from the collinear periodic orbit crossed each other in a homoclinic point at higher energy. These branches are not invariant if flux across them.

Davis' resolution led us to understand how a trajectory behaves when TST is exact in phase space. There is a single periodic orbit which guides the flux in and out through its respective separatrix branches. Reactive trajectories start outside the separatrices will stay outside in order to cross the barrier only once and never return. Those trajectories start in between the separatrices will stay inside and do not react. However, when there are multiple periodic orbits violated the single TS, Davis resolved an interaction region where neither reactive trajectories enter nor nonreactive ones stay there forever. This kind of trajectories can have the same total energy, but they may differ in their partitioning and their initiated channels. Based on these criteria, new techniques are developed via a surface of sections.

Armed with the previous knowledge that the PODS obey the concept of "points of no return "in the forward direction shown in Chapter 4, we shall elucidate a phase space region in the backward time direction. The SSPO neighbourhood is adequately studied by Davis, who concluded that their separatrices would be invariant even at slightly higher

energy such that they are not intersected. Our goal is to follow the linearised trajectories on the stable manifold emanating from F_1 collinear periodic orbit in backwards. Note that trajectories started nearby the periodic orbits are distorted off their orbital rotation. The process is to follow an ensemble of trajectories very near the stable manifold of F_1 until they cross a surface of section located at the DS. An advantage of this is that when a trajectory starts on a stable manifold, it will stay within the stable manifold for probably long backward time. The above discussion is strictly valid with area-preserving maps of fixed points which could be a projected periodic orbit. Another benefit is that an invariant stable manifold can separate reactive from nonreactive trajectories. This is also unarguably true once the stable manifold does not be crossed by an unstable manifold.

Allahem *et al* [41] found some trajectories that lay close enough to the boundary of the main nonreactive layer of the DS which gave rise to periodic motions as they pass by the periodic orbit F_1 in the product side. As shown in Figure 5.1, many trajectories generates the stable intersection appear to rotate around the F_1 in backaward of time. Rotation can make difference between trajectories landed on different layers as plotted in Figure 5.2. It can be seen a trajectory starts on the boundary of inner layer has more trips around F_1 than ones start on the boundary of the main nonreactive layer.

The location of a trajectory and the time direction is taken to help us to see the whole picture in phase space. Because there are unstable periodic orbits on both sides of the SSPO (due to reflection symmetry) that drive the flow to the reaction zone where complexity occurs.

Compared to chaotic scattering system where the potential energy of a particle more magnificent than the total energy of the Hamiltonian system, our scattering region is partly chaotic which is created by the intersection of the stable and unstable manifolds of F_1. This region is called the homoclinic region where an orbit interacted with the scattering in the homoclinic tangle then leaves to an asymptote area. Hereafter, we will discuss the relationship between inputs σ used to generates the initial conditions used for the un/stable intersections with the time of intersections. Such a piece in Figure 5.3 is called an icicle that shows how far trajectories located very near F_1 and

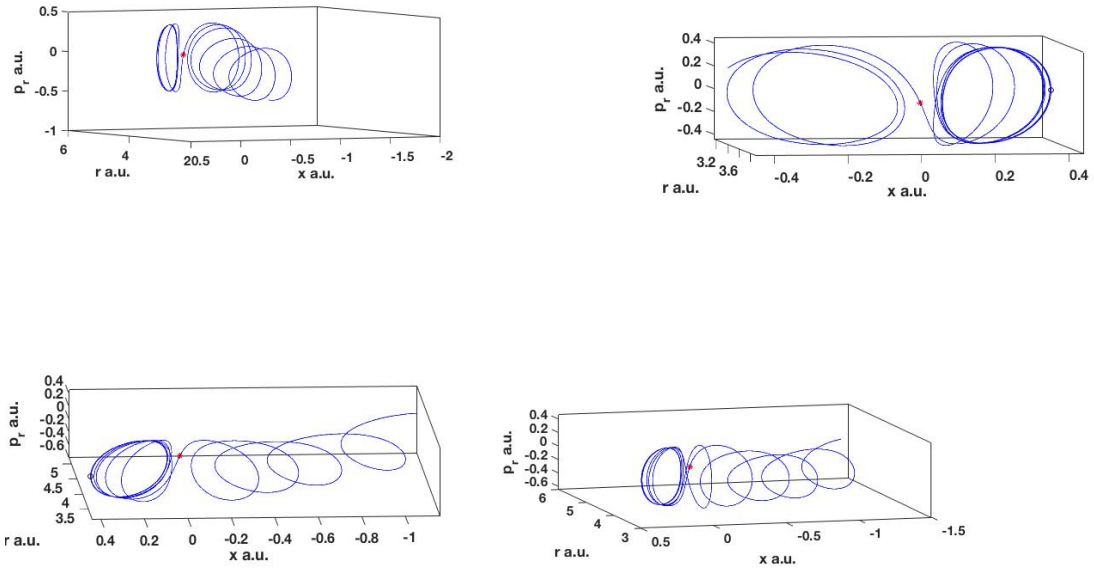

FIGURE 5.1: *Trajectories chosen on the stable intersection emanated from the F_1. Time direction is backward and red sign is the DS. Direction of horizontal axis is modified to show the periodic motion.*

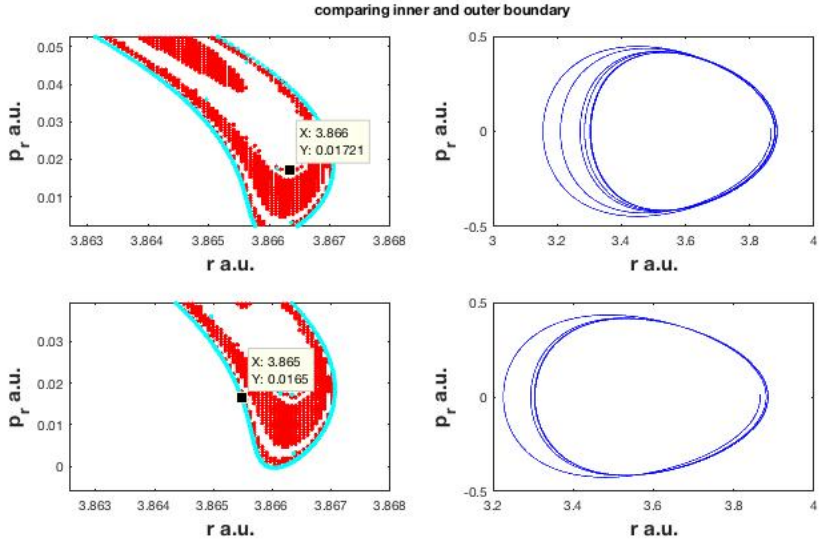

FIGURE 5.2: *Trajectories chosen on the inner and outer layers as shown on the left pannel.*

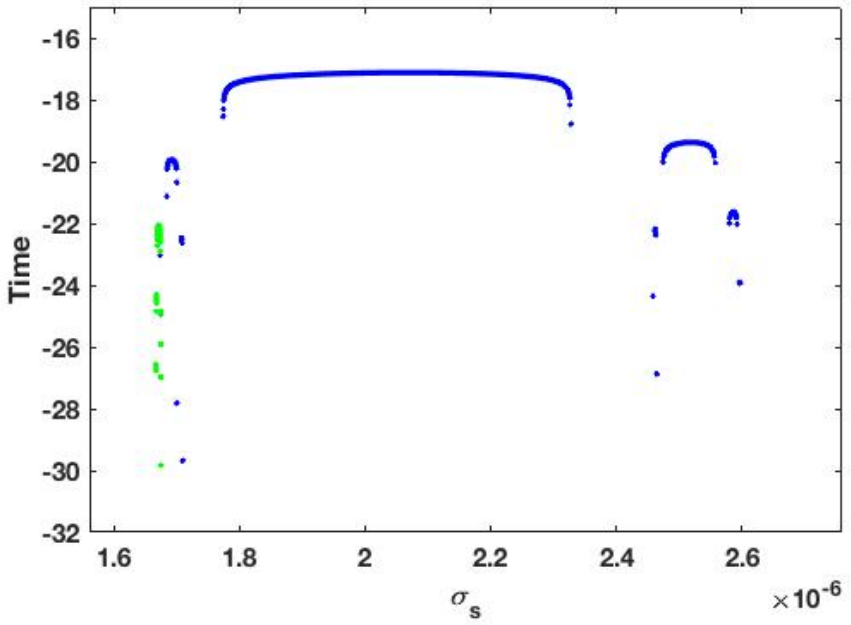

FIGURE 5.3: There are in most icicle plots σ_s refers to deviation from the stable manifold where succeed trajectories cross the DS such that blue colour stand for outer and green colour for inner boundary. Note that there are no more icicles in the gaps.

cross the DS in particular backward time. The generation of icicles extends to negative infinity from the central icicle, which creates the chattering region. These icicles are smooth subdomain which separated by a region of more complicated behaviour [101]. An obvious explanation can be seen with the help of the Figure 5.3 where each blue icicle represents those trajectories lie on the boundary of the main layer. However, green icicles represent those trajectories creating the inner boundary which spend less time than those creating the outer main boundary.

Now, we shall narrow the search to find out which of these fractal icicles shall be the best in the sense that low distribution results in more points on the stable intersection found in Chapter 4 or even in the previous study.

The central icicle is the best to represent the stable intersection which can be shown in Figure 5.4. An important thing to consider is that as more σ used to generate more

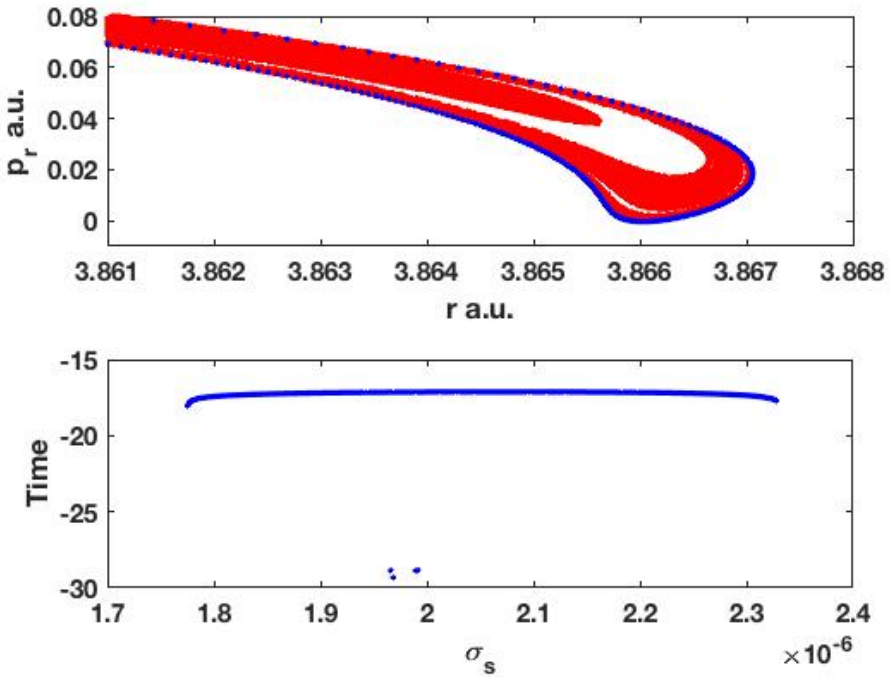

FIGURE 5.4: The best icicle create the stable intersection that lies on the boundary of the main nonreactive island as shown in the top panel.

initial conditions on the central icicle, newly separated icicles start to appear on both sides of the central icicle as shown in Figure 5.3. These additional new icicles are located more closely to F_1 than the central icicle and then have fewer rotations' trips around F_1 before distorting from the periodic orbit in order to across the DS. Having said that those icicles located significantly closer to the F_1 should cross the DS at the boundary of the inner layers which differ based on time-consuming during rotation. However, the top right icicle of the central icicle shown in Figure 5.5 generate the stable intersection but with more distributed points.

How about choosing σ_s between two icicles? Through the numerical experiment, it shows no trajectory crosses the DS. Moreover, Figure 5.6 shows those trajectories lay on the part of the stable intersection, which does not cover the whole boundary due to low distribution.

Finding σ_s between either trajectory that succeeds to cross the DS or those trajectories do not cross the DS is not an easy task. However, we found that at $\sigma_s = 8.071201315 \times$

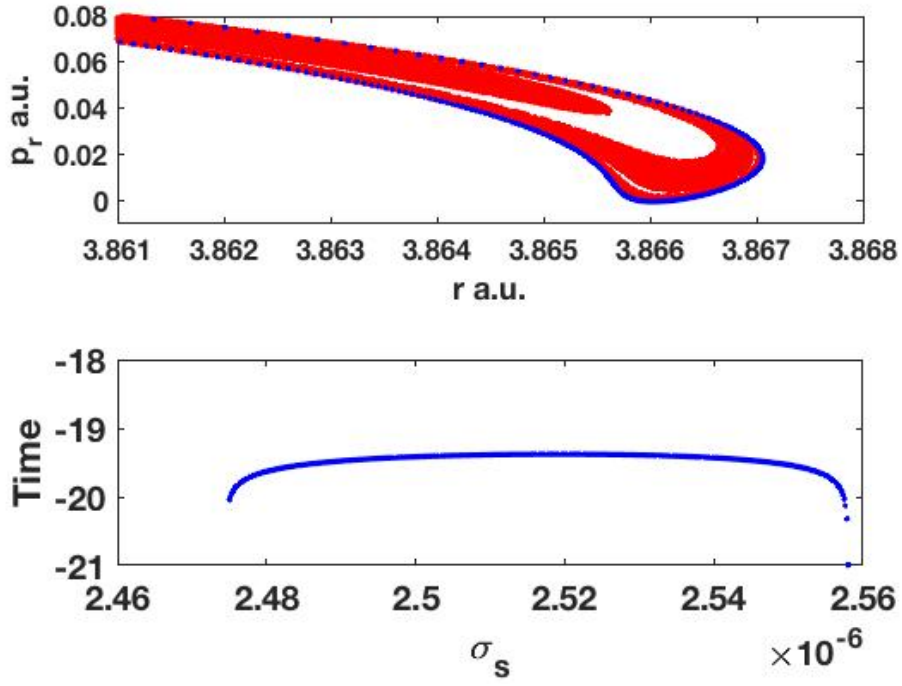

FIGURE 5.5: The top right icicle of the central icicle generates points in the stable intersection that lies randomly on the boundary of the main nonreactive island as shown in the top panel.

10^{-7} located between $\sigma_s \in [8.07119978 \times 10^{-7}, 8.071205647 \times 10^{-7}]$ the trajectory is not crossing the DS. As more σ_s is generated inside the icicle and trajectories propagated on the linear approximation of the stable manifold backwards in time in which Figure 5.8 is shown. Most trajectories cross the Poincaré surface of the section (PSS) located at SSPO at the boundary of the main nonreactive layer. While some of them cross the PSS at different layers' boundaries, moreover, repeating propagating succeed trajectories will not provide an inner boundary for the inner layers.

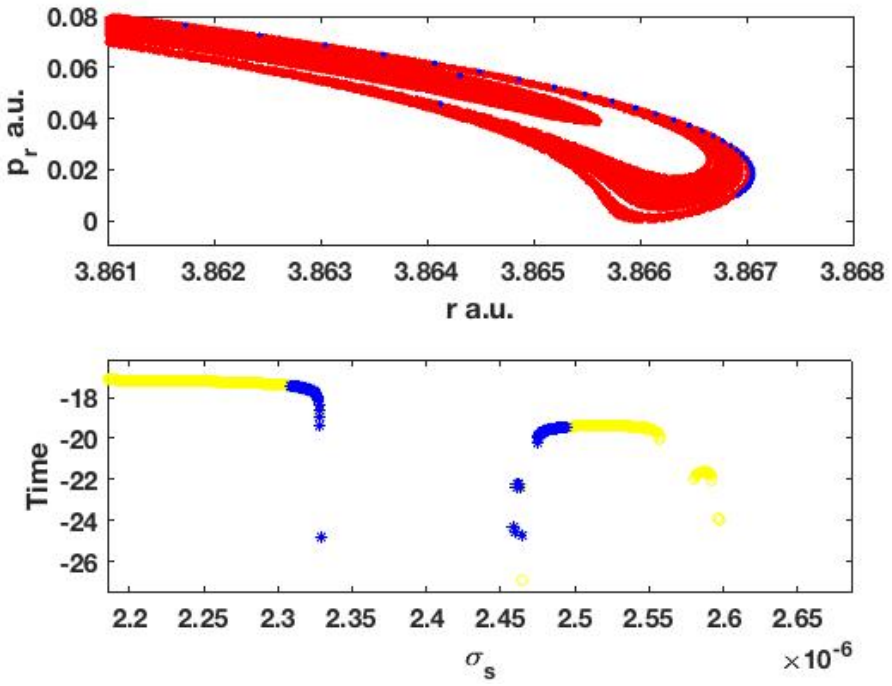

FIGURE 5.6: The region of complicated behaviour between the best icicle and the top right icicle as shown in blue colour.

5.3 Recrossing Phenomena

In this section, we will shed light on the crossing phenomena and check if it is connected to each layer on the reactive islands of the DS. Note that the reactive term is adapted to a transmitted trajectory meaning product in the future evolution of reactant in the past while the nonreactive term redefined to those trajectories react and recross the DS before being reflected back to their reactants or products asymptote. This is useful when we compare the DS in the past and in future propagation.

Before that, we shall give reviews of history and theory.

The appreciation of the work done by Pechukas *et al* [21] and [30] help us to understand the dynamics near the saddle point and solved the recrossing problem for a range of energies in 2dof. Even though their work was remarkable in configuration space, extending the VTST to phase space is essential to address the more dimensional severe problem.

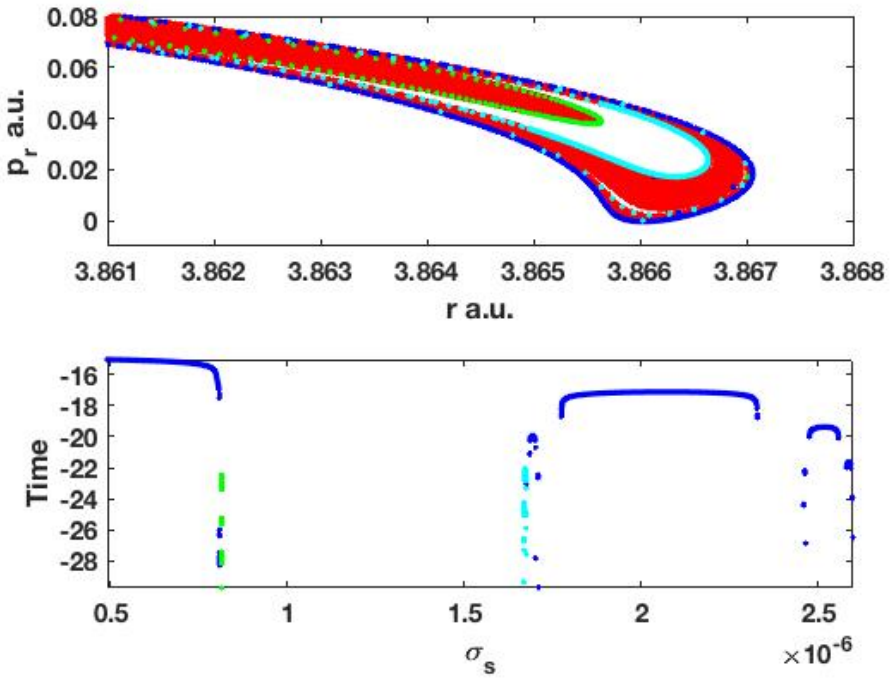

FIGURE 5.7: The inner boundaries are shown with the outer boundary on top as well as their icicles down.

Most recently, Uzer and co-workers [36] provide an excellent piece of work to extend the concept of a DS beyond the configuration space.

Our approach is based on the Poincaré surface of section. The surface of section can be generated for the collinear system with two dof by initiating trajectories at $x = 0$ and propagating them in phase space and plotting r, and p_r coordinates whenever the x coordinate recrossed again such that p_x is positive.

Recrossing detection is apparently dependent on the numerical tolerance is chosen and computer power used. When the TST is exact, trajectories are expected to cross the PSS once and only once in forward time direction at low energy. One can predict if a reflected trajectory started at the product side, it would return back in its future evolution.

The phase space structure at $E = -4.141$ e.V. is firstly considered for many reasons. There are five periodic orbits, including the symmetric stretch. Besides the symmetric

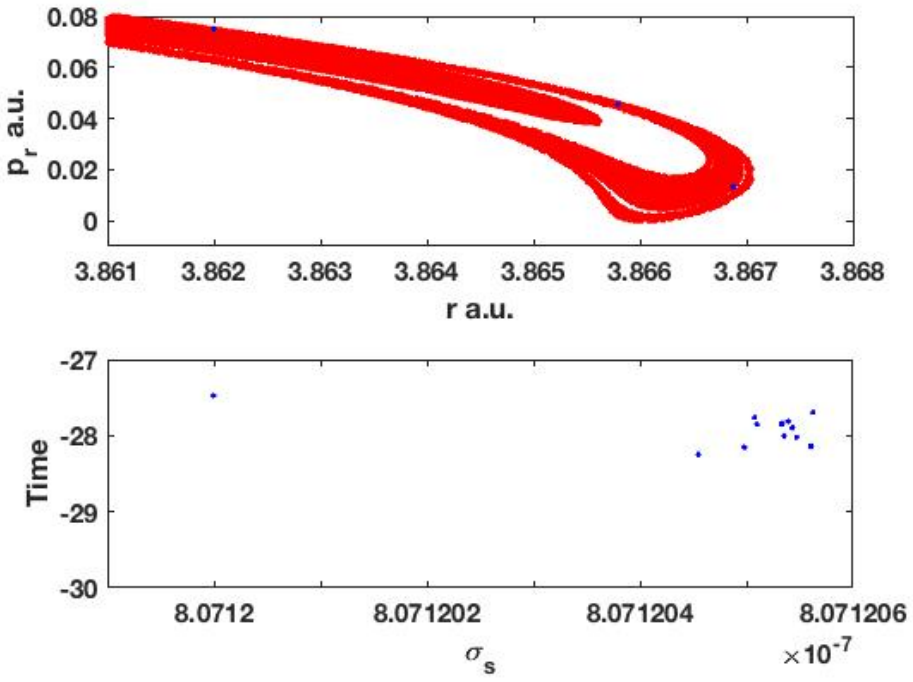

FIGURE 5.8: Generating more data on the interval explain in text in more detail.

stretch periodic orbit, other periodic orbits occur symmetrically at both sides of the saddle point and have already reported by many authors. Such the complex behaviour has been reported by Davis [57] and most recently, by Iñarrea *et al* [20].

Plot in Figure 5.9 shows an ensemble of 16161 trajectories that are generated on the DS and propagated forward in time direction in order to recross the surface of section ($x = 0$) before leaving to either reactant or product sides.

The ensemble of trajectories plot is based on their initial points and time direction evolution where the colour scheme is varied according to the number of the intersection points. Blue colour indicates transmitted trajectories with more than two intersections. While yellow colour shows transmitted trajectories with one intersection and green colour refers to transmitted trajectories with two intersections. Note that transmitted trajectories here refer to those trajectories that leave to the product side while reflected trajectories return back to their reactant region. The similar indication would be shown for reflected trajectories with one intersection (cyan) and two intersections in magenta colour, as well

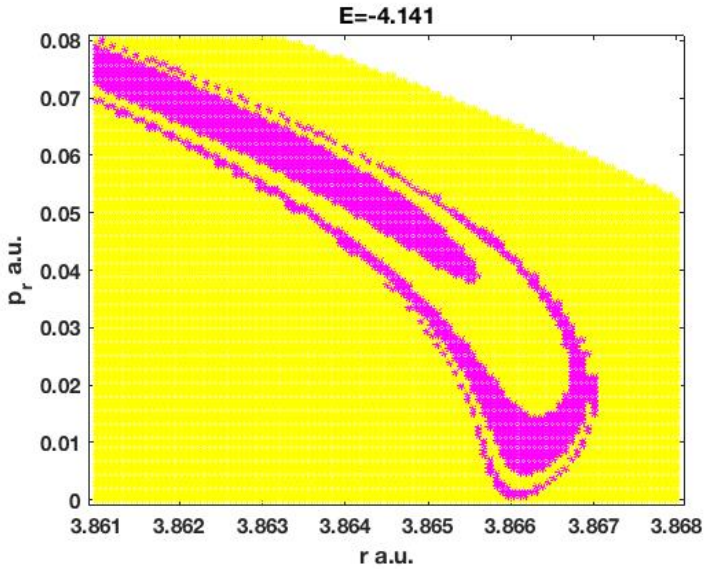

FIGURE 5.9: Part of the DS in forward time direction.Yellow shows crossing once while magenta for two times crossing. Energy in e.V.

as red colour, refers to more than two intersections. In Figure 5.9, reflected trajectories record two crossings for each trajectory. The maximum time for a trajectory to cross the DS is about 9.45 a.u at $E = -4.141$ e.V.

The overall picture can be seen in plot Figure 5.10 where two different ensembles have been chosen before and after first nonreactive trajectory appeared on the reactive islands. The DS at $E = -4.15$ eV. is filled by only reactive trajectories. Another ensemble of $E = -4.0$ eV. can be seen in Figure 5.10 where recrossing events occur with transmitted trajectories shown in blue. A similar colour scheme is used as before to indicate the number of intersecting points for reflected ensemble in the forwards.

Since the Hamiltonian system has time-reversal symmetry, it is worth to show how trajectories propagated in the past evolution. This will be shown for energy value $E = -4.141\, eV.$ with a similar colour scheme as before. The plot of the same ensemble used in Figure 5.9 shows trajectories propagated backwards in the time direction. As before similar colour scheme used and indicates that cyan represent reflected trajectories and green refers to transmitted ones in Figure 5.11. The nonreactive droplets appear in

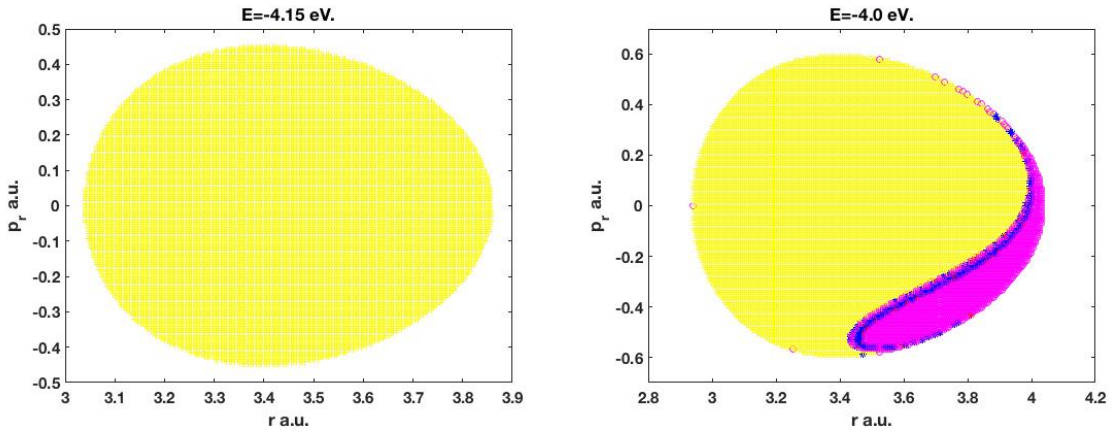

FIGURE 5.10: The DS in forward time direction.Yellow shows crossing once while blue for more than two in reactive islands. Magenta refers to two crossings and red for more than two times crossing in the nonreactive islands. The text has more descriptor detail.

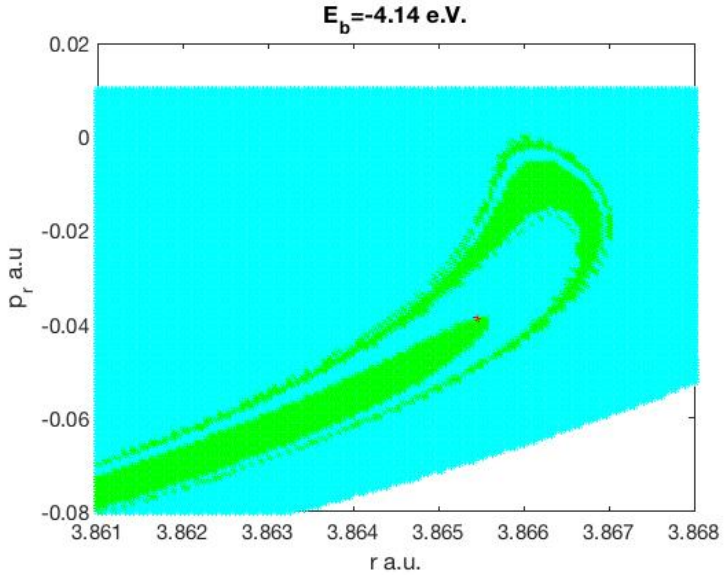

FIGURE 5.11: The DS in backward time direction. Green shows transmitted trajectories recross twice while cyan for reflected ones cross the DS only once and red for more than two for reflected one.

the past DS where transmitted trajectories recross the PSS twice compared to reflected trajectories with one time crossing.

The emergence of nonreactive droplets on the past DS are symmetric to those in forward DS, as shown in Figure 5.11. These droplets are related to the forward DS in Figure 5.9

TABLE 5.1: Crossing numbers. t_b and t_f refer to backward and forward time direction respectively. tra refers to transmitted trajectories while $ref.$ refers to reflected trajectories.

E eV.	Input	Max tra.	Min tra.	Max ref.	Min ref.	Max time	Min time	Output
-4.141 t_b	16161	2	2	1	1	9.45	0	16168
-4.141 t_f	16161	1	1	2	2	9.45	0	16168
-4.0 t_f	16134	5	1	6	2	15.5	6.61	18410
-4.15 t_f	15037	1	1	0	0	0	0	15037

by time-invariant reversal symmetry. Therefore, not only the collinear periodic orbit F_1 causes the appearance of nonreactive droplets but also the mirror image of the F_1 has been involved. These droplets consist of an ensemble of trajectories that are reactive, as stated by Davis for energy where the TST is exact. However, recrossing detection shows that these droplets include those trajectories with many time crossing.

Table 5.1 displays the number of crossing for various computed trajectories on the DS at different energy values. The table shows transmitted and reflected trajectories maximum and minimum crossing number and also maximum (minimum) time spent by a trajectory to cross the dividing surface at each energy value declared. Also, the input total of trajectories with the total output intersected points are declared. The table also illustrates a single intersection point for each trajectory propagated forward at lower energy than the bifurcation threshold. Above that, each transmitted trajectory cross the PSS once as they propagated forward at $E = -4.141$ e.V. Contrary to these transmitted trajectories, reflected trajectories record even times crossing in their future evolution while it shows either none recrossing at low energy or one time at higher energy when they are propagated backwards in time. This means that the DS gives an exact TST at low energy, and the numerical calculation cannot be a reason for the TST failure.

5.4 Invariant Manifolds of the Collinear Periodic Orbit

In this section, we will provide a review of theoretical and appreciating the structure of the stable and unstable manifolds of the collinear periodic orbit F_1. As described in Chapter 4, these manifolds generate a stable intersection on the DS. This section is self-contained and provides a detailed mathematical discussion and ideas developed by many participants. However, emphasis focus on the contribution of Poincaré and Smale. For more details, the reader refers to [102], [66] and Holmes [103] for an excellent review. Of course, the greatest contribution can be seen in the texts of [104] and [105].

First, we will start by providing a theory developed by Poincaré for the restricted many problems. His approach is based on geometric and qualitative ideas which were extended in a topological way by Birkhoff and Smale.

The methods Poincaré used is used to reduce a two dof Hamiltonian system to a time-dependent system with a single degree of freedom. The procedure contains two main results, including the Hamiltonian integral and time replaced by timelike coordinate. Therefore, we will describe the method briefly in general Hamiltonian as follows:

Since the Hamiltonian is time-independent, the derivative with respect to time implies the Hamiltonian is conservative energy. Therefore, one can solve the Hamiltonian for one coordinate as a function of the constant energy h and the remaining three coordinates as:

$$p_1 = p_1(q_1, q_2, p_2; h). \tag{5.1}$$

Then, one can replace the time by other coordinates say q_1. So, the coordinate q_1 becomes a time-like independent variable. In this way, time is eliminated in favour of q_1, but it can reproduce after solving the reduced system. Thus, we retain the geometry of the solution, and the solution can be seen in terms of the dependent variables q_2 and p_2, the constant energy and the independent variable q_1.

Now, we can write the reduced Hamiltonian system in terms of the new independent variable and use p_1 from 5.1 in order to have the reduced Hamiltonian system as follows:

$$\frac{dq_2}{dq_1} = g(q_2, p_2; q_1; h)$$
$$\frac{dp_2}{dq_1} = f(q_2, p_2; q_1; h). \tag{5.2}$$

Clearly, the original Hamiltonian system is reduced to a q_1-dependent , single degree of freedom system. Since the new system is Hamiltonian,

$$\hat{H} := -p_1(q_2, p_2; q_1; h),$$

one can solve the reduced Hamiltonian system in order to reproduce the full solution back up through the definitions.

Now, we shall submit these definitions to our collinear Hamiltonian system and define a proper crossing surface of section in order to use for the discovery of asymptote manifolds associated with the periodic orbit F_1.

5.4.1 The Un/Stable Manifolds

In this section, we will appreciate the structure formed by the manifolds of F_1, which help to understand the dynamic on the energy surface by means of a surface of section.

As explained in the literature, invariant manifolds are cylinders on the energy surface. These cylinders are of codimension one of the energy surface, and if they intersect with the surface of section, they will produce lines divided the energy surface into two disjoint parts. However, if stable and unstable manifolds of F_1 do intersect, they do not act as separatrix or barrier because flux will flow across them from one cylinder to another one. This situation is understood as nonreactive trajectories appeared on the DS while some transmitted ones have to recross the DS many times at higher energy shown in Chapter 4.

In general, the linear approximation suggests how to approximate the stable intersection generated by the stable manifold of F_1 in equation (4.1). One may reverse the simulation in order to determine the stable manifold. This can be followed by propagating trajectories of the linearization of the hyperbolic point $x_* \in F_1$ in the forward time direction in order to across a proper surface of section defined below.

Ultimately, we require to define a crossing sectional surface that is transverse to the flow of the collinear system and then intersected by all trajectories such that the Hamiltonian is smooth. Note that, an attempt to separate rotational from vibrational dof will result in vibrational phase space as explained in Chapter —refChapter3. Therefore, single dof Hamiltonian is not going to be efficient and may break the smoothness condition of the map–P. As a result, we will solve the full system in order to retain the global manifolds from the map at a fixed point.

Let us define the surface of section by $p_r = 0, \dot{p_r} > 0$ and construct a return map P associated with the first intersection in the following setting: every point (x, p_x) on the map has been chosen such that r is a solution to the Hamiltonian function

$$H(0, p_x, r, x) = E$$

whereas the energy is conserved and $x = x_*$. These points can be counted as the first intersection on the surface. By choosing $p_r > 0$, every point (x, p_x) is mapped to the next intersection with solution at T time step, $(p_r(T), p_x(T), r(T), x(T))$ in forward time direction to determine the unstable manifold and vice versa for the stable manifold of F_1. These points are expected to intersect the surface of the section in orders because the energy is fixed.

Figure 5.12 shows these (second) intersections are easy to observe in the forward time direction. The backward time direction can be obtained by applying time-reversal invariance symmetry to the result obtained by the forwards or to the initial conditions with negative momenta and then propagate them in backwards as the second iteration counted. Clearly, that first intersection assumed to be on the return map constructed

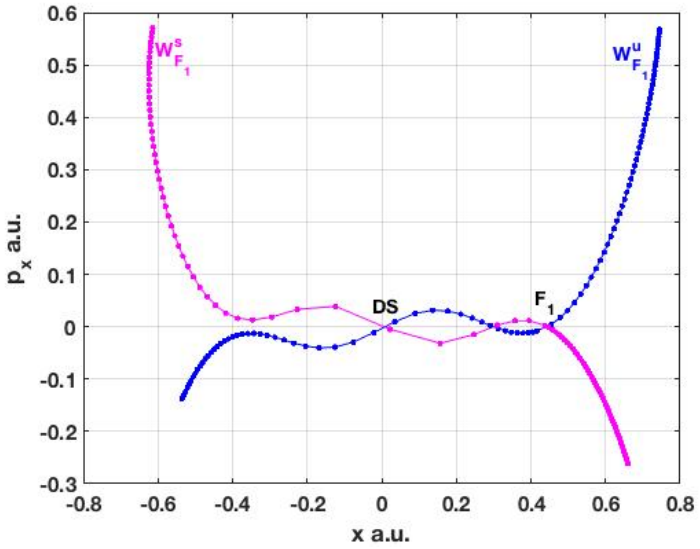

FIGURE 5.12: Phase space regions divided by the stable $W^s(x_*)$ and unstable $W^u(x_*)$ manifolds of F_1 as shown magenta for backwards and blue for forwards calculations.

and the second intersection observed when the trajectories return by the map P in forward time for the unstable manifold and backwards for the stable one. This Figure also shows these intersection points on both manifolds asymptote to the fixed point.

If the Hamiltonian is autonomous and the flow is reversible, the return map P^{-1} can be obtained.

If the system is periodic in p_1, then the trajectory returns to the surface S at a point say s after time 2π. In this way, the flow of the dynamical system can be studied under the Hamiltonian $\hat{H}$ to a study of a discrete Poincaré map, $P : S \to S$.

If the Hamiltonian $\hat{H}$ is smooth, then the map P will be orientation preserving. Because the flow under $\hat{H}$ is Hamiltonian and preserve volume, the area is preserved by the map$P$.

When aperiodic orbit returns to the surface, it will intersect the surface in a single point. This is the fixed point of the map P such that $P(p) = p$. Determining the stability of P is under the iteration of the map. Then, one can compute the linearization of the map at a fixed point. Thus, the linearization is a linear map to itself under $DP(p)$ which is

the monodromy matrix. If their eigenvalues such that

$$|\lambda_s| < 1 > |\lambda_u|,$$

Then, the fixed point is hyperbolic. Assume we define the linear spaces, E^s and E^u by computing the eigenvectors associated with eigenvalues of the monodromy matrix of a hyperbolic point. Thus, the linear spaces are invariant under the flow of the linearisation map, $DP(p)$. The stable manifolds theorem for maps stats that, there exist local invariant manifolds W^s_{loc} and W^u_{loc}, in a neighbourhood of p of the fully nonlinear map. The local manifolds are tangential to the linear spaces at p and as smooth as the P–map. Finally, iterating points on each of the local manifolds reveal the global unstable and stable manifolds.

Clearly, these approximated manifold associated with the hyperbolic point, cannot self–intersect, otherwise, the P–map will not be smooth. However, the two asymptotic manifolds may intersect each other in the so-called homoclinic point. In this situation, a single homoclinic point implies infinity many intersections because it lies on both manifolds. Repeated iteration of the map reveals an infinite number of intersections.

Geometrically, we start to envision that the unstable manifold of F_1 will intersect with the stable manifold of F_1 as the points of intersection asymptote toward the periodic point. The resulting dynamics coincide with Smale's horseshoe map [106] where the unstable manifold have to extend back across the stable manifold which shrinks back asymptote to the periodic points. Similarly, the stable manifold will have to double back across the unstable manifold in the backward time since the map is orientation preserving.

Another way is to linearise the full system by generating an ensemble of trajectories using the identity given in (4.1) and propagate them backwards in time to across the surface of section similar to that used for the P–map. Every point on the linear approximation will be mapped to intersect the surface of the section in backward time direction for the asymptotic stable manifold of the periodic point, similarly for the asymptotic unstable manifold of F_1. Figure 5.13 shows the stable and unstable manifolds of the linearization

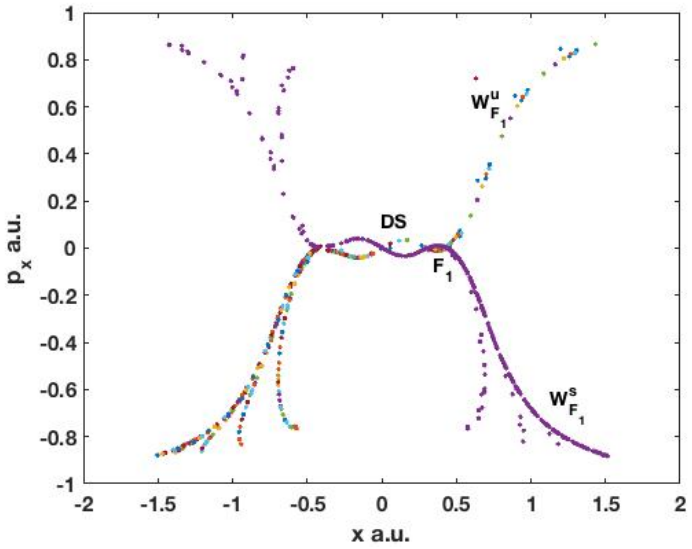

FIGURE 5.13: The un/stable manifolds of F_1 are presented by the linear approximation where $W^s(x_*)$ represent the stable manifold of F_1 and $W^u(x_*)$ refer to the unstable manifold similar to what the return map does.

of the periodic point. The critical point is that the linearization preserves the structure as the map P does.

Chapter 6

Conclusion

In this thesis, we have discussed the phase space structure of the collinear hydrogen reaction. Though, the phase space structure is already investigated at low energy for such reaction, that the system must pass through the symmetric stretch periodic orbit which represents the DS separating reactants from products region, the transition structure remains unclear at higher energy where the dynamics transit to chaos. This study is an extension to a recent work of Allahem [41] particularly because of the simple configuration to the hydrogen reacted on the Porter–Karplus potential energy surface. His approach is based on the stable manifold of the collinear periodic orbit F_1 which intersects the DS and bounds the main nonreactive layer emerged on the DS at a particularly high energy. It should also state that the present approach can generate a result with much better agreement with reactive islands simulation and provide boundaries for various nonreactive layers on all versions of the forward DS. These layers arise on the backward DS and can be bounded by the symmetric stable and unstable intersections easily as on all investigated versions of the forward hemispheres.

Though, the previous work provides an important pathway and insight guide to current study, All attempts in here have employed similar techniques and ideas used also in nonlinear dynamics. The present approach yields much better understanding than most recent approaches centred in the DS. Neither the theory of manifold nor computer power was adequate to explore the phase space structure cause the system to be more chaotic.

It should also state that those are the manifolds associated with the additional periodic orbit lie in the collinear system. With the help of previous work, we figure out those manifolds associated with a couple of symmetric additional periodic orbits, which led the nonreactive droplets opened up in the forward hemisphere of the DS. Those are the stable manifold in the product side and the unstable manifold of the mirror image periodic orbit in the reactant region.

In the collinear reaction, the methods require more effort and time to implement such manifolds. Therefore, we make use of the symmetry inherited in the system to find one by another. It should also state that the intersection of stable and unstable manifolds of the collinear unstable orbit yields chaotic behaviour by means of chaotic scattering, discussed in Chapter 5. Reactive islands and linear approximation methods are merged to understanding and bounding such nonreactive droplets in the DS. All methods used a proper Poincaré surface of sections based on our purpose and the location of the symmetric stretch periodic orbit. Recrossing issues are recognised at the DS at higher energies while at low energy shows one-time crossing. It shows numerical calculation cannot be a reason for nonreactive IC's appeared on the DS. It should state that it is better to locate the surface of section far away from the region of complexity where those involved collinear orbits invalidated the calculation.

In this thesis, we showed the stable and unstable manifolds of the additional periodic orbit which must cause the TST to break in phase space. Our representation is based on the latest knowledge that they are intersecting each other before even crossing the DS and leading the system to be more chaotic. In fact, these results make it obvious in order to explicit the long-sought structure for the 2 dof system inherited symmetry property. It should state that only the stable manifold of the F_1 change the structure of the forward hemisphere while the unstable manifold of the mirror image F_1' cause the nonreactive droplets to appeared on another version of the forward hemisphere. It should note that linear approximation is carefully agreed with P-map generating IC's in the vicinity of F_1 and propagated forward or backwards to across a surface of section for appreciating both manifolds.

This research has raised interesting questions for both theoretical and applied reaction disciplines. Some of them are anticipated and discussed in the last section 5.4 of Chapter 5 in order to present such manifolds. It would be extremely important to find a good normal form approximation for representing the intersected manifolds in the case of symmetric systems. Some useful information can be taken up in future work to extend the present idea to even higher energies values in the current collinear hydrogen exchange reaction or the full system with three degrees of freedom. Naturally, it would be reasonable to know whether our idea and attempts can be used to study other reactive systems with asymmetric configuration.

Bibliography

[1] W. H. Miller. Spiers memorial lecture: Quantum and semiclassical theory of chemical reaction rates. *Faraday Discuss. Chem. Soc.*, 110:1–21, 1998. doi: 10.1002/9780470141601.ch35. URL http://dx.doi.org/10.1002/9780470141601.ch35.

[2] W. H. Miller. Beyond transition-state theory: a rigorous quantum theory of chemical reaction rates. *Acc. Chem. Res.*, 26(4):174–181, 1993. doi: 10.1021/ar00028a007. URL http://pubs.acs.org/doi/abs/10.1021/ar00028a007.

[3] Holger Waalkens, Roman Schubert, and Stephen Wiggins. Wigner's dynamical transition state theory in phase space: classical and quantum. *Nonlinearity*, 2007.

[4] William H Miller. "direct" and "correct" calculation of canonical and microcanonical rate constants for chemical reactions. *The Journal of Physical Chemistry A*, 1988.

[5] Gabor Jancso and W Alexander Van Hook. Condensed phase isotope effects. *Chemical Reviews*, 74(6):689–750, 1974.

[6] AR Ubbelohde and KJ Gallagher. Acid-base effects in hydrogen bonds in crystals. *Acta Crystallographica*, 8(2):71–83, 1955.

[7] Samuel Glasstone, Henry Eyring, and Keith J Laidler. *The theory of rate processes*. McGraw-Hill, 1941.

[8] J Hirschfelder, Henry Eyring, and Nathan Rosen. I. calculation of energy of h3 molecule. *The Journal of Chemical Physics*, 1936.

[9] George E Kimball and John G Trulio. Quantum mechanics of the h3 complex. *The Journal of Chemical Physics*, 1958.

[10] SF Boys and I Shavitt. A fundamental calculation of the energy surface for the system of three hydrogen atoms. *NTIS, Springfield, VA, AD212985*, 1959.

[11] F. London. Zur Theorie und Systematik der Molekularkräfte. *Zeitschrift für Physik*, 63(3-4):245–279, 1930. doi: 10.1007/BF01421741. URL http://dx.doi.org/10.1007/BF01421741.

[12] Shin Sato. Potential energy surface of the system of three atoms. *The Journal of Chemical Physics*, 1955.

[13] R. N. Porter and M. Karplus. Potential energy surface for H_3. *J. Chem. Phys.*, 40: 1105, 1964. doi: 10.1063/1.1725256. URL http://link.aip.o/JCP/40/1105/1.

[14] Donald G Truhlar and Charles J Horowitz. Functional representation of liu and siegbahn's accurate abinitio potential energy calculations for h+ h2. *The Journal of Chemical Physics*, 1978.

[15] P Siegbahn and B Liu. An accurate three-dimensional potential energy surface for h3. *The Journal of Chemical Physics*, 1978.

[16] Antonio JC Varandas, Franklin B Brown, C Alden Mead, Donald G Truhlar, and Normand C Blais. double many-body expansion of the two lowest-energy potential surfaces and nonadiabatic coupling for h3. *The Journal of Chemical Physics*, 1987.

[17] NC Blais and DG Truhlar. High-energy collision-induced dissociation of h2 by h. *The Astrophysical Journal*, 1982.

[18] Toshiyuki Takayanagi, Nobuyuki Masaki, Kazutaka Nakamura, Makoto Okamoto, Shin Sato, and George C Schatz. The rate constants for the h+ h2 reaction and its isotopic analogs at low temperatures: Wigner threshold law behavior. *The Journal of chemical physics*, 1987.

[19] A. I. Boothroyd, W. J. Keogh, P. G. Martin, and M. R. Peterson. An improved H_3 potential energy surface. *J. Chem. Phys.*, 95(6):4343–4359, 1991. doi: http://

dx.doi.org/10.1063/1.461758. URL http://scitation.aip.org/content/aip/journal/jcp/95/6/10.1063/1.461758.

[20] M. Iñarrea, J.F. Palacián, A.I. Pascual, and J.P. Salas. Bifurcations of dividing surfaces in chemical reactions. *J. Chem. Phys.*, 135:014110, 2011. doi: 10.1063/1.3600744. URL http://link.aip.org/link/JCP/135/014110/1.

[21] P. Pechukas and F. J. McLafferty. On transition-state theory and the classical mechanics of collinear collisions. *J. Chem. Phys.*, 58(4):1622–1625, 1973. doi: 10.1063/1.1679404. URL http://link.aip.org/link/JCP/58/1622/1.

[22] D. G. Truhlar, W. L. Hase, and J. T. Hynes. Current status of transition-state theory. *J. Phys. Chem.*, 87(15):2664–2682, July 1983. doi: 10.1021/j150644a044. URL http://cdn-pubs.acs.org/doi/abs/10.1021/j150644a044.

[23] B. C. Garrett D. G. Truhlar and S. J. Klippenstein. Current status of transition-state theory. *J. Phys. Chem.*, 100(31):12771–12800, August 1996. doi: 10.1021/jp953748q. URL http://pubs.acs.org/doi/abs/10.1021/jp953748q.

[24] E. Pollak and P. Talkner. Reaction rate theory: What it was, where it is today, and where is it going? *Chaos*, 15(2):026116, June 2005. doi: 10.1063/1.1858782. URL http://link.aip.org/link/CHA/15/026116/1.

[25] A. Marcelin. Contribution à l'étude de la cinétique physico-chimique. *Annales de Physique*, 3:158, 1915.

[26] H. Eyring and M. Polanyi. Über einfache Gasreaktionen. *Zeitschrift für Physikalische Chemie B*, 12:279, 1931.

[27] R. S. Mackay, J. D. Meiss, and I. C. Percival. Transport in Hamiltonian systems. *Physica D: Nonlinear Phenomena*, 13(1–2):55 – 81, 1984. ISSN 0167-2789. doi: http://dx.doi.org/10.1016/0167-2789(84)90270-7. URL http://www.sciencedirect.com/science/article/pii/0167278984902707.

[28] R. S. Mackay, J. D. Meiss, and I. C. Percival. Resonances in area-preserving maps. *Physica D: Nonlinear Phenomena*, 27(1–2):1 – 20, 1987. ISSN 0167-2789. doi: http://dx.doi.org/10.1016/0167-2789(87)90002-9. URL http://www.sciencedirect.com/science/article/pii/0167278987900029.

[29] P. Pechukas. *Statistical approximations in collision theory*, volume 2. Springer, 1976. doi: 10.1007/978-1-4757-0644-4_6. URL http://dx.doi.org/10.1007/978-1-4757-0644-4_6. edited by W. H. Miller.

[30] P. Pechukas. Transition state theory. *Annual Review of Physical Chemistry*, 32 (1):159–177, 1981. doi: 10.1146/annurev.pc.32.100181.001111. URL http://www.annualreviews.org/doi/abs/10.1146/annurev.pc.32.100181.001111.

[31] E. Pollak and P. Pechukas. Transition states, trapped trajectories, and classical bound states embedded in the continuum. *J. Chem. Phys.*, 69:1218, 1978. doi: 10.1063/1.436658. URL http://link.aip.org/link/JCP/69/1218/1.

[32] P Pechukas. Dynamics of molecular collisions. *Part*, 2:269, 1976.

[33] E. Pollak and P. Pechukas. Unified statistical model for complex and direct reaction mechanisms: A test on the collinear $H_2 + H$ exchange reaction. *J. Chem. Phys.*, 70:325, 1979. doi: 10.1063/1.437194. URL http://link.aip.org/link/JCP/70/325/1.

[34] M. J. Davis. Phase space dynamics of bimolecular reactions and the breakdown of transition state theory. *J. Chem. Phys.*, 86:3978, 1987. doi: 10.1063/1.451908. URL http://link.aip.org/link/JCP/86/3978/1.

[35] S. Wiggins. *Normally hyperbolic invariant manifolds in dynamical systems*, volume 105. Springer, 1994. doi: 10.1007/978-1-4612-4312-0.

[36] T. Uzer, C. Jaffé, J. F. Palacián, P. Yanguas, and S. Wiggins. The geometry of reaction dynamics. *Nonlinearity*, 15(4):957, 2002. URL http://stacks.iop.org/0951-7715/15/i=4/a=301.

[37] M. J. Davis and S. K. Gray. Unimolecular reactions and phase space bottlenecks. *J. Chem. Phys.*, 84:5389, 1986. doi: 10.1063/1.449948. URL http://link.aip.org/link/JCP/84/5389/1.

[38] A. Allahem and T. Bartsch. Chaotic dynamics in multidimensional transition states. *J. Chem. Phys.*, 137(21):214310, 2012. doi: 10.1063/1.4769197. URL http://link.aip.org/link/JCP/137/214310/1.

[39] H. Waalkens, A. Burbanks, and S. Wiggins. Phase space conduits for reaction in multidimensional systems: HCN isomerization in three dimensions. *J. Chem. Phys.*, 121(13):6207–6225, October 2004. doi: 10.1063/1.1789891. URL http://link.aip.org/link/JCP/121/6207/1.

[40] H. Waalkens, A. Burbanks, and S. Wiggins. Escape from planetary neighbourhoods. *Mon. Not. R. Astron. Soc.*, 361(3):763–775, August 2005. doi: 10.1111/j.1365-2966.2005.09237.x. URL http://dx.doi.org/10.1111/j.1365-2966.2005.09237.x.

[41] Ali Allahem. *Numerical investigation of chaotic dynamics in multidimensional transition states*. PhD thesis, © Loughborough University, 2014.

[42] W. H. Miller, Y. Zhao, M. Ceotto, and S. Yang. Quantum instanton approximation for thermal rate constants of chemical reactions. *J. Chem. Phys.*, 119(3):1329–1342, 2003. doi: 10.1063/1.1580110. URL http://link.aip.org/link/JCP/119/1329/1.

[43] C. B. Li, M. Toda, and T. Komatsuzaki. Bifurcation of no-return transition states in many-body chemical reactions. *J. Chem. Phys.*, 130:124116, 2009. doi: 10.1063/1.3079819. URL http://link.aip.org/link/JCP/130/124116/1.

[44] R. S. MacKay and D. C. Strub. Bifurcations of transition states: Morse bifurcations. *ArXiv e-prints*, May 2013. URL arxiv.org/abs/1305.1967.

[45] H. P. de Oliveira, A. M. Ozorio de Almeida, I. Damião Soares, and E. V. Tonini. Homoclinic chaos in the dynamics of a general Bianchi type-IX model. *Phys.*

Rev. D, 65:083511, Apr 2002. doi: 10.1103/PhysRevD.65.083511. URL http://link.aps.org/doi/10.1103/PhysRevD.65.083511.

[46] C. Jaffé, D. Farrelly, and T. Uzer. Transition state theory without time-reversal symmetry: Chaotic ionization of the hydrogen atom. *Phys. Rev. Lett.*, 84:610–613, Jan 2000. doi: 10.1103/PhysRevLett.84.610. URL http://link.aps.org/doi/10.1103/PhysRevLett.84.610.

[47] C. Jaffé and T. Uzer. Direct and chaotic ionization in the presence of external fields: the transition-state theory point of view. *J. Phys. Chem. A*, 105(12):2783–2791, 2001. doi: 10.1021/jp0038761. URL http://pubs.acs.org/doi/abs/10.1021/jp0038761.

[48] C. Jaffé, S. D. Ross, M. W. Lo, J. Marsden, D. Farrelly, and T. Uzer. Statistical theory of asteroid escape rates. *Phys. Rev. Lett.*, 89:011101, Jun 2002. doi: 10.1103/PhysRevLett.89.011101. URL http://link.aps.org/doi/10.1103/PhysRevLett.89.011101.

[49] B. Eckhardt. Transition state theory for ballistic electrons. *Journal of Physics A: Mathematical and General*, 28(12):3469, 1995. URL http://stacks.iop.org/0305-4470/28/i=12/a=019.

[50] Komatsuzaki T. and Berry R. S. Regularity in chaotic reaction path $I : Ar_6$. *J. Chem. Phys.*, 110:9160, 1999. doi: 10.1063/1.478838. URL http://link.aip.org/link/JCP/110/9160/1.

[51] K. J. Laidler and M. C. King. Development of transition-state theory. *J. Phys. Chem.*, 87(15):2657–2664, 1983. doi: 10.1021/j100238a002. URL http://pubs.acs.org/doi/abs/10.1021/j100238a002.

[52] F. J. McLafferty and P. Pechukas. Quantum transition state theory. *Chem. Phys. Lett.*, 27(4):511 – 514, 1974. ISSN 0009-2614. doi: 10.1016/0009-2614(74)80293-9. URL http://www.sciencedirect.com/science/article/pii/0009261474802939.

[53] S. Chapman, S. M. Hornstein, and W. H. Miller. Accuracy of transition state theory for the threshold of chemical reactions with activation energy. Collinear and three-dimensional atomic hydrogen + molecular hydrogen. *J. Am. Chem. Soc.*, 97(4):892–894, 1975. doi: 10.1021/ja00837a035. URL http://pubs.acs.org/doi/abs/10.1021/ja00837a035.

[54] C. Jaffé, S. Kawai, J. Palacián, P. Yanguas, and T. Uzer. A new look at the transition state: Wigner's dynamical perspective revisited. *Adv. Chem. Phys.*, 130A:171–216, January 2005. doi: 10.1002/0471712531.ch3. URL http://dx.doi.org/10.1002/0471712531.ch3.

[55] E. Pollak. *Theory of Chemical Reaction Dynamics*, volume 3. CRC Press, Boca Raton, FL, 1985. edited by M. Baer.

[56] M. J. Davis. Bottlenecks to intramolecular energy transfer and the calculation of relaxation rates. *J. Chem. Phys.*, 83:1016, 1985. doi: 10.1063/1.449465. URL http://link.aip.org/link/JCP/83/1016/1.

[57] M. J. Davis. Phase space structure in classically chaotic regions and the nature of quantum eigenstates. *J. Phys. Chem.*, 92(11):3124–3144, 1988. doi: 10.1021/j100322a024. URL http://pubs.acs.org/doi/abs/10.1021/j100322a024.

[58] A. Tiyapan and C. Jaffé. Classical atom-diatom scattering: Self-similarity, scaling laws, and renormalization. *J. Chem. Phys.*, 99(4):2765–2780, August 1993. doi: 10.1063/1.465185. URL http://link.aip.org/link/JCP/99/2765/1.

[59] A. Tiyapan and C. Jaffé. Classical S-matrix theory for chaotic atom-diatom collisions. *J. Chem. Phys.*, 101(12):10393–10403, December 1994. doi: 10.1063/1.467920. URL http://link.aip.org/link/JCP/101/10393/1.

[60] A. Tiyapan and C. Jaffé. Chaotic scattering: An invariant fractal tiling of phase space. *J. Chem. Phys.*, 103(13):5499–5511, October 1995. doi: 10.1063/1.465185. URL http://link.aip.org/link/JCP/99/2765/1.

[61] Komatsuzaki T. and Nagaoka M. A dividing surface free from a barrier recrossing motion in many-body systems. *Chem. Phys. Lett.*, 265:91, 1997. doi: http://dx.

doi.org/10.1016/S0009-2614(96)01414-5. URL http://www.sciencedirect.com/science/article/pii/S0009261496014145.

[62] Tamiki Komatsuzaki and R Stephen Berry. Chemicalreactiondynamics: Many-bodychaosandregularity. *Advances in Chemical Physics*, 149:79, 2003.

[63] Komatsuzaki T. and Berry R. S. Regularity in chaotic reaction path II : Ar_6 -energy dependence and visualization of the reaction bottleneck. *Phys. Chem. Chem. Phys.*, 1:1387, 1999. doi: 10.1039/A809424A. URL http://dx.doi.org/10.1039/A809424A.

[64] Komatsuzaki T. and Berry R. S. Local regularity and non-recrossing path in transition states: A new strategy in chemical reaction theories. *J. Mol. Struct. (Theochem)*, 506:55, 2000. doi: http://dx.doi.org/10.1016/S0166-1280(00)00402-4. URL http://www.sciencedirect.com/science/article/pii/S0166128000004024.

[65] H. Goldstein. *Classical mechanics*, volume 4. Pearson Education India, 1962.

[66] S. Wiggins. *Introduction to applied nonlinear dynamical systems and chaos*, volume 2. Springer, 2003. doi: 10.1007/b97481.

[67] A. Litvak-Hinenzon and V. Rom-Kedar. Resonant tori and instabilities in hamiltonian systems. *Nonlinearity*, 15(4):1149, 2002. URL http://stacks.iop.org/0951-7715/15/i=4/a=310.

[68] R. Continenti. *Vibrational State-Resolved Differential Cross Section for the* $D + H_2 \rightarrow DH + H$ *Reaction.* PhD thesis, University of California, Berkeley, November 1989.

[69] E. H. Taylor and S. Datz. Study of chemical reaction mechanisms with molecular beams. the reaction of K with HBr. *J. Chem. Phys.*, 23(9):1711–1718, 1955. doi: 10.1063/1.1742417. URL http://link.aip.org/link/JCP/23/1711/1.

[70] P. Brumer and M. Karplus. Perturbation theory and ionic models for alkali halide systems. II. Dimers. *J. Chem. Phys.*, 64:5165, 1976. doi: 10.1063/1.432191. URL http://link.aip.org/link/JCP/64/5165/1.

[71] S. A. Buntin, C. F. Giese, and W. R. Gentry. State-resolved differential cross sections for the reaction $D + H_2 \rightarrow HD + H$. *J. Chem. Phys.*, 87:1443, 1987. doi: 10.1063/1.453275. URL http://link.aip.org/link/JCP/87/1443/1.

[72] G. W. Johnston, B. Katz, K. Tsukiyama, and R. Bersohn. Isotopic variants of the atomic hydrogen+ hydrogen reaction. 1. Total reaction cross sections of the atomic hydrogen+ deuterium and atomic hydrogen+ hydrogen deuteride reactions as a function of relative energy. *J. Phys. Chem.*, 91(21):5445–5451, 1987. doi: 10.1021/j100305a013. URL http://pubs.acs.org/doi/abs/10.1021/j100305a013.

[73] M. Born. Born-Oppenheimer approximation. *Ann. Phys*, 84:457–484, 1927. URL http://gallica.bnf.fr/ark:/12148/bpt6k15386r.

[74] Mikhail Lemeshko, Roman V Krems, John M Doyle, and Sabre Kais. Manipulation of molecules with electromagnetic fields. *Molecular Physics*, 2013.

[75] Shuwu Xu, Yunhua Yao, Chenhui Lu, Jingxin Ding, Tianqing Jia, Shian Zhang, and Zhenrong Sun. Manipulating field-free molecular alignment by v-shaped femtosecond laser pulses. *Physical Review A*, 2014.

[76] Benjamin J Sussman. Five ways to the nonresonant dynamic stark effect. *American Journal of Physics*, 2011.

[77] Giacinto Scoles, Davide Bassi, Udo Buck, and Derek Laine. *Atomic and molecular beam methods*. Oxford university press New York, 1988.

[78] Bretislav Friedrich and Dudley R Herschbach. Spatial orientation of molecules in strong electric fields and evidence for pendular states. *Nature*, 1991.

[79] HJ Loesch and A Remscheid. Brute force in molecular reaction dynamics: A novel technique for measuring steric effects. *The Journal of Chemical Physics*, 1990.

[80] Philip J Bustard, R Lausten, and Benjamin J Sussman. Molecular alignment and orientation with a hybrid raman scattering technique. *Physical Review A*, 2012.

[81] Markus Kurz and Peter Schmelcher. Ultralong-range rydberg molecules in combined electric and magnetic fields. *Journal of Physics B: Atomic, Molecular and Optical Physics*, 2014.

[82] Philip J Bustard, Guorong Wu, Rune Lausten, Dave Townsend, Ian A Walmsley, Albert Stolow, and Benjamin J Sussman. From molecular control to quantum technology with the dynamic stark effect. *Faraday discussions*, 2011.

[83] R. G. Littlejohn and M. Reinsch. Gauge fields in the separation of rotations and internal motions in the n-body problem. *Rev. Mod. Phys.*, 69(1):213–275, January 1997. doi: 10.1103/RevModPhys.69.213. URL http://dx.doi.org/10.1103/RevModPhys.69.213.

[84] R. G. Littlejohn, K. A. Mitchell, V. Aquilanti, and S. Cavalli. Body frames and frame singularities for three-atom systems. *Phys. Rev. A*, 58(5):3705–3717, Nov 1998. doi: 10.1103/PhysRevA.58.3705. URL http://link.aps.org/doi/10.1103/PhysRevA.58.3705.

[85] H. Waalkens and S. Wiggins. Geometrical models of the phase space structures governing reaction dynamics. *Regular and Chaotic Dynamics*, 15(1):1–39, 2010. ISSN 1560-3547. doi: 10.1134/S1560354710010016. URL http://dx.doi.org/10.1134/S1560354710010016.

[86] P. Pechukas and E. Pollak. Classical transition state theory is exact if the transition state is unique. *J. Chem. Phys.*, 71:2062, 1979. doi: 10.1063/1.438575. URL http://link.aip.org/link/JCP/71/2062/1.

[87] E. Pollak, M. S. Child, and P. Pechukas. Classical transition state theory: a lower bound to the reaction probability. *J. Chem. Phys.*, 72:1669, 1980. doi: 10.1063/1.439276. URL http://link.aip.org/link/JCP/72/1669/1.

[88] Krajňák V. *Phase Space Geometry and Invariant Manifolds Underlying Reaction Dynamics*. PhD thesis, University of Bristol, 2017.

[89] C. C. Marston and N. De Leon. Reactive islands as essential mediators of unimolecular conformational isomerization: A dynamical study of 3-phospholene.

J. Chem. Phys., 91(6):3392–3404, 1989. doi: 10.1063/1.456914. URL http://link.aip.org/link/JCP/91/3392/1.

[90] N. De Leon and C. C. Marston. Order in chaos and the dynamics and kinetics of unimolecular conformational isomerization. *J. Chem. Phys.*, 91(6):3405–3425, 1989. doi: 10.1063/1.456915. URL http://link.aip.org/link/JCP/91/3405/1.

[91] Cleve B Moler. *Experiments with MATLAB*. Society for Industrial and Applied Mathematics, 2011.

[92] Ying-Cheng Lai and Tamás Tél. *Transient chaos: complex dynamics on finite time scales*. Springer Science & Business Media, 2011.

[93] Edward Ott. *Chaos in dynamical systems*. Cambridge university press, 2002.

[94] Charles Jean Joachain. *Quantum collision theory*. 1975.

[95] CC Rankin and William H Miller. Classical s matrix for linear reactive collisions of h+ cl 2. *The Journal of Chemical Physics*, 55(7):3150–3156, 1971.

[96] Kiyohiko Someda, Ramakrishna Ramaswamy, and Hirok Nakamura. Decoupling surface analysis of classical irregular scattering and clarification of its icicle structure. *The Journal of chemical physics,AIP*, 1993.

[97] Siegfried Bleher, Celso Grebogi, and Edward Ott. Bifurcation to chaotic scattering. *Physica D: Nonlinear Phenomena*, 1990.

[98] Christof Jung and Peter H Richter. Classical chaotic scattering-periodic orbits, symmetries, multifractal invariant sets. *Journal of Physics A: Mathematical and General*, 1990.

[99] David K Campbell. Chaos/xaoc. soviet-american perspectives on nonlinear science. *Chaos/XAOC. Soviet-American perspectives on nonlinear science., by Campbell, DK. American Institute of Physics, New York, NY (USA), 1990, 512 p., ISBN 0-88318-778-7,*, 1990.

[100] Ying-Cheng Lai, Tamás Tél, and Celso Grebogi. Stabilizing chaotic-scattering trajectories using control. *Physical Review E*, 1993.

[101] R Guantes, F Borondo, and S Miret-Artés. Periodic orbits and the homoclinic tangle in atom-surface chaotic scattering. *Physical Review E*, 56(1):378, 1997.

[102] John Guckenheimer and George Buzyna. Dimension measurements for geostrophic turbulence. *Phys. Rev. Lett.*, 51:1438–1441, 1983.

[103] John Guckenheimer and Philip Holmes. *Nonlinear oscillations, dynamical systems, and bifurcations of vector fields*, volume 42. Springer Science & Business Media, 2013.

[104] Henri Poincaré. New methods of celestial mechanics. *Springer Science & Business Media*, 13, 1992.

[105] Stephen Smale. Differentiable dynamical systems. *Bulletin of the American mathematical Society*, 73(6):747–817, 1967.

[106] Morris W Hirsch, Stephen Smale, and Robert L Devaney. *Differential equations, dynamical systems, and an introduction to chaos*. Academic press, 2012.